

On the consistent and scalable detection of spatial patterns

Jiayu Su^{1,2,3#}, Jun Hou Fung^{1,2}, Haoyu Wang^{2,4}, Dian Yang^{2,4}, David A. Knowles^{2,3,5#}, and Raul Rabadan^{1,2,6#}

¹*Program for Mathematical Genomics, Columbia University, New York, NY, USA*

²*Department of Systems Biology, Columbia University, New York, NY, USA*

³*New York Genome Center, New York, NY, USA*

⁴*Department of Molecular Pharmacology and Therapeutics, Columbia University, New York, NY, USA*

⁵*Department of Computer Science, Columbia University, New York, NY, USA*

⁶*Department of Biomedical Informatics, Columbia University, New York, NY, USA*

Abstract

Detecting spatial patterns is fundamental to scientific discovery, yet current methods lack statistical consensus and face computational barriers when applied to large-scale spatial omics datasets. We unify major approaches through a single quadratic form and derive general consistency conditions. We reveal that several widely used methods, including Moran’s I, are inconsistent, and propose scalable corrections. The resulting test enables robust pattern detection across millions of spatial locations and single-cell lineage-tracing datasets.

Keywords Spatial statistics, Spatial variability, Moran’s I, Single-cell lineage tracing

1 Main

Since Hooke’s first microscopic glimpses of cellular structure in 1665, scientific progress has relied on the recognition of spatial patterns. The rapid rise of spatial omics¹ has given this task new urgency: platforms now measure tens of thousands of molecular features simultaneously, rendering manual inspection infeasible and fueling an explosion of computational methods for detecting spatially variable genes (SVGs)^{2–7} and beyond⁸. Yet benchmarking studies^{9–12} reveal a fragmented landscape where methods disagree and performance varies unpredictably, with no principled explanation for these discrepancies. Furthermore, current tools struggle to keep pace with technological maturation; few, if any, can scale to modern datasets comprising millions of locations. In this work, we address these challenges through theoretical unification and general algorithmic acceleration. We demonstrate that virtually all major SVG detection approaches—including Moran’s I¹³, parametric models, and non-parametric tests—are mathematically equivalent instances of a single quadratic-form test (*Q-test*), differing primarily in their choice of spatial kernel. This recasts spatial variability detection as a problem of kernel spectrum design, revealing general consistency conditions that explain when and why methods succeed or fail and stripping the computational requirements down to their first-principles essentials.

We begin by formulating pattern detection as a general dependency testing problem (Figure 1a). Under the null hypothesis of independent and identically distributed (i.i.d.) measurements, we derive a test statistic $Q_n = \mathbf{z}^\top \mathbf{K} \mathbf{z}$, where \mathbf{z} denotes standardized observations and \mathbf{K} encodes spatial structure (Supplementary Note 2). By evaluating score statistics at the null, we show that common regression-based SVG tests reduce asymptotically to this same form. We further link Q_n to the distributional distance between the joint and factorized marginal distributions, connecting it to dependence measures such as the Hilbert-Schmidt Independence Criterion (HSIC)¹⁴ and Kullback-Leibler divergence. Importantly, our analysis challenges a previous categorization¹¹ where methods labeled “kernel-free” are not kernel-free in a mathematical sense (Supplementary Note 1). Graph-based statistics such as Moran’s I rely on the adjacency matrix, while dependence-based approaches typically introduce kernels implicitly through density estimation.

This unification allows us to rigorously diagnose test consistency—that is, the ability to reliably detect any pattern as the number of profiled locations increases. We prove that all Q-tests are limited to

#Correspondence: js5756@cumc.columbia.edu; dak2173@columbia.edu; rr2579@cumc.columbia.edu

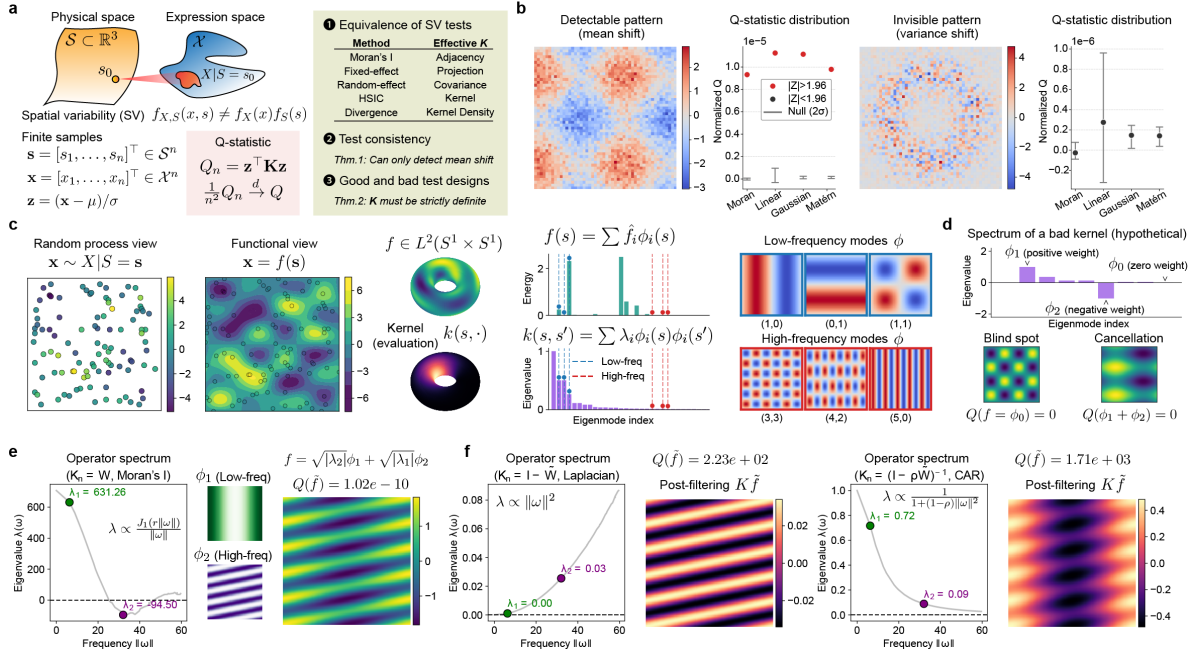


Figure 1: Theoretical analysis of spatial variability tests. (a) Summary of main theoretical results. (b) Q-test can only detect mean-shift patterns (left); variance shifts (right) remain invisible. (c) Spatial patterns can be modeled as deterministic functions in a Hilbert space decomposable into a frequency basis. The discrete kernel matrix converges to an integral operator with a corresponding spectral decomposition. (d) A hypothetical kernel spectrum illustrating two sources of false negatives: “blind spots” (signal aligns with the kernel’s null space) and “cancellation” (signal energy is split between positive and negative eigenvalues summing to zero). (e) Spectral cancellation of Moran’s I. The adjacency kernel with a fixed distance cutoff has an indefinite and oscillatory spectrum. (f) Graph Laplacian and its inverse (CAR) enforce strict definiteness, resolving cancellation but restricting sensitivity to high or low frequency regimes.

detecting mean-shift patterns (Theorem 1; Figure 1b). While higher-order dependencies are theoretically undetectable by Q_n , they are empirically indistinguishable from pure mean shifts due to the single-observation-per-location constraint of spatial omics. We therefore adopt a functional perspective, treating spatial patterns as deterministic elements of a Hilbert space that can be expanded in a frequency basis (Supplementary Note 3; Figure 1c). Under this view, we prove a test is consistent if and only if the kernel is strictly definite (Theorem 2; Figure 1d). Indefinite kernels, including the adjacency matrix in Moran’s I, suffer from spectral cancellation: signals aligned with eigenmodes of opposite sign offset one another, producing false negatives even for strong signals (Figure 1e).

Among consistent Q-tests, no single kernel is universally optimal. Because scaling is irrelevant, prioritizing one frequency naturally necessitates trivializing others. For instance, the Graph Laplacian¹⁵ targets sharp, localized changes of high frequencies, while its inverse (the conditional autoregressive, or CAR¹⁶, kernel) targets smooth, broad-scale trends of low frequencies (Figure 1f). Combining the two can broaden sensitivity but inevitably dilutes power at the extremes. In practice, it is common to favor smooth spatial patterns while maintaining a heavy spectral tail to capture potentially interesting local variation, motivating the polynomial decay of Matérn and CAR kernels¹⁷. Spectra can also be learned from data implicitly through neural networks, though this requires care to avoid overfitting and does not guarantee superior detection (Supplementary Note 3.5.2). Finally, not all kernels are computationally efficient for datasets scaling to millions of locations. We introduce two accelerations to address this (Online Methods). For general geometries, we optimize the CAR kernel via implicit matrix–vector products and Hutchinson’s trace estimator¹⁸ to avoid dense kernel matrices (Figure S1a–b). For grids, we leverage the Toeplitz structure to compute the quadratic form via fast Fourier transforms, reducing complexity from $O(N^3)$ to $O(N \log N)$ for all kernels while accurately approximating the spectrum (Figure S1c; Figure S2a). These techniques enable SVG detection on one million spots in under one second—orders of magnitude faster and more memory-efficient than existing implementations (Figure S2b).

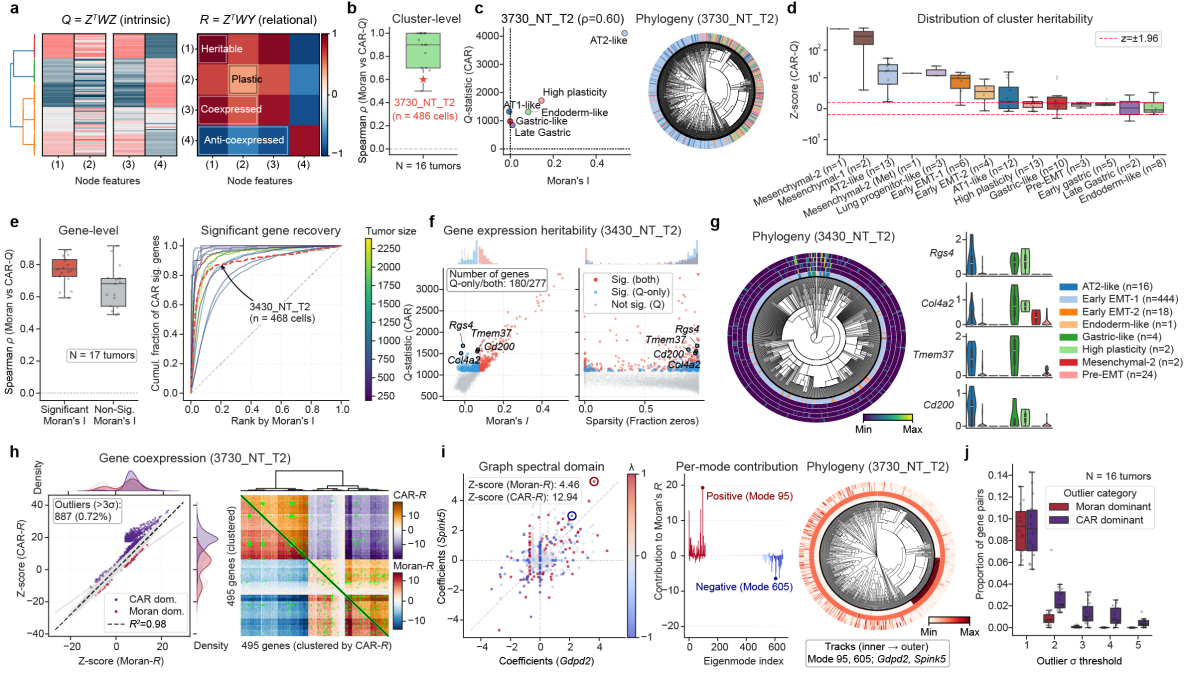


Figure 2: Detecting heritability and plasticity in tumor lineage tracing data. (a) Schematic of intrinsic (Q) and relational (R) pattern detection showing four hypothetical genes: (1) heritable (phylogeny-aligned); (2) plastic (unaligned); (3) co-expressed with (1); and (4) anti-coexpressed with (1). (b) Cluster-level heritability concordance (Spearman ρ between Moran's I and CAR- Q) across 16 tumors. (c) Cell-state heritability in tumor 3730_NT_T2 showing Q -statistic comparison (left) and tumor phylogeny (right). (d) Distribution of cell-state heritability Z-scores (CAR- Q) across tumors. Red dashed lines indicate significance thresholds ($Z = \pm 1.96$). (e) Gene-level performance heritability concordance. Left: correlation of test statistics for genes stratified by Moran's I significance ($p\text{-val} < 0.05$). Right: cumulative recovery curves showing fraction of CAR-significant genes ($p\text{-val} < 0.05$) recovered when ranked by Moran's I in decreasing order. (f) Gene expression heritability (left) and sparsity (right) in tumor 3430_NT_T2. Red: genes significant by both methods; blue: significant only by CAR ($p\text{-val} < 0.05$). (g) Log-normalized expression of discordant genes from (f). Left: phylogeny with tracks showing cell-state annotation and log-normalized expression (inner to outer: *Rgs4*, *Col4a1*, *Tmem37*, *Cd200*). Right: expression distributions by cell state. (h) Bivariate co-expression analysis. Left: Z-scores (Moran- R vs. CAR- R) of gene pairs with regression outliers highlighted. Right: heatmap of gene modules clustered by CAR- R ; green boxes indicate outlier pairs. (i) Spectral decomposition of a discordant gene pair (*Spink5*, *Gdpd2*). Left: graph spectral coefficients. Middle: eigenmode contribution to Moran's R showing cancellation between Mode 95 (red, positive) and Mode 605 (blue, negative). Right: phylogeny showing log-normalized expression of both genes and the two eigenmodes. (j) Proportion of method-specific outlier gene pairs across varying outlier thresholds (σ). Boxplots in b, d, e, g, j show median (center line), interquartile range (box), and 1.5× interquartile range (whiskers).

Since biological variation is rarely random, theoretical limitations in spatial pattern detection may not always manifest in real data. To assess the practical implications, we designed a gene-ranking experiment using noise-corrupted patterns and found Moran's I to be the least robust, particularly at low expression levels (Figure S2c). Similarly, in a mouse small intestine Visium HD dataset¹⁹, Moran's I diverged from other kernel methods in the top variable genes, a discrepancy driven primarily by low-expression features (Figure S2d–e). Leveraging the scalability of our implementation, we also illustrate the value of multi-resolution comparison. For instance, the “Swiss roll” pattern introduced during sample preparation was preferentially detected at 8 μm resolution due to signal dampening at the 16 μm Nyquist limit (Figure S2f–g). Finally, we evaluated Moran's R²⁰, the bivariate counterpart to Moran's I often used for spatial co-expression²¹ (Online Methods). Despite sharing similar theoretical vulnerabilities, these limitations primarily reduce detection power through magnitude attenuation while preserving gene-pair rankings (Figure S2h). The resilience likely stems from the fact that high-frequency patterns are rare in real spatial transcriptomics and typically lack the magnitude required to fully cancel out low-frequency biological signals.

Beyond physical space, our framework generalizes to single-cell data by assessing variability over similarity graphs⁵. On such application is the characterization of expression heritability along a single-cell tumor phylogenetic tree. Here, low-frequency patterns correspond to stable gene programs inherited from a common ancestor and maintained across offspring, while high-frequency variation within the same branch implies plasticity²² (Figure 2a). To uncover these patterns, we analyzed a lung cancer lineage tracing dataset characterized by irregular and sparse clones²³ (Online Methods). At the cell-state level, Moran's I and the CAR kernel show high concordance, as rankings were driven by strong clustering signals detectable by both (Figure 2b–c). Across tumors, we recapitulated known heritability patterns for each cell state (Figure 2d). At the gene level, Moran's I exhibited a high false-negative rate (Figure 2e). Closer examination revealed that it failed to detect markers for rare subclones because sparse signals were obscured by high-frequency intra-clone variation (Figure 2f–g). In contrast, the CAR kernel, which is by design robust to such local fluctuations, reliably identified these heritable programs. Finally, in bivariate co-expression analysis, the same spectral limitations of Moran's R caused false negatives in detecting co-regulated modules (Figure 2h–j).

In summary, we establish the theoretical cohesion for spatial pattern detection and identify kernel spectrum as the key statistical ingredient. We show that classic metrics like Moran's I suffer from spectral cancellation—a flaw that, while subtle in spatial data, causes persistent signal loss and false negatives in graph-based analyses. To resolve this, we propose an efficient correction using the low-pass CAR kernel. Combined with our scalable open-source implementation, this work provides the mathematically sound foundation necessary for reliable pattern detection across the expanding landscape of spatial omics and beyond.

2 Online Methods

2.1 Unification of spatially variable gene tests.

Consider a feature vector $\mathbf{x} \in \mathbb{R}^n$ observed at locations $\mathbf{s} \in \mathcal{S}^n$. Under the null hypothesis of no spatial variability, we standardize the data to \mathbf{z} such that $\mathbb{E}[\mathbf{z}] = \mathbf{0}$ and $\text{Var}(\mathbf{z}) = \mathbf{I}$. We demonstrate that the test statistics for a broad class of spatial methods—including fixed effect models, Linear Mixed Models (LMM), Generalized Linear Mixed Models (GLMM), graph-based and other non-parametric dependence tests—are asymptotically equivalent to a general quadratic form $Q_n = \mathbf{z}^\top \mathbf{K} \mathbf{z}$ (Supplementary Note 2). This common structure reveals a shared theoretical limitation: these tests are consistent only against alternatives of *mean dependence*, defined as $\mathbb{E}[X|S] \neq \mathbb{E}[X]$. Because they rely on a quadratic form of the first moments, they are theoretically blind to higher-order dependencies, such as pure changes in spatial variance (Theorem 1, Supplementary Note 2).

The Q-statistic framework allows us to systematically examine how different modeling assumptions influence test properties and final results. In fixed-effect models, \mathbf{K} acts as a projection matrix onto spatial basis functions, whereas in random-effect models (LMMs), it represents the spatial covariance matrix. Generalized models (GLMs and GLMMs) fit within this framework by adjusting the standardized vector \mathbf{z} according to the mean-variance relationship defined by the link function; here, non-Gaussian distributions introduce gene-specific scaling factors that typically increase sensitivity for highly expressed genes. For graph-based methods, \mathbf{K} corresponds to the adjacency or Laplacian matrix. Finally, in dependence-based frameworks, the kernel either characterizes the space of spatial patterns (as in HSIC) or arises from density estimation in divergence metrics. The implications of these design choices are detailed in Supplementary Note 3.

2.2 Kernel spectral analysis and consistency under the functional view.

Under the single-observation-per-location constraint, we analyze the consistency of the Q-test by modeling observations \mathbf{x} as samples from a deterministic function $f(\mathbf{s})$. In the large-sample limit ($n \rightarrow \infty$), the discrete statistic converges to the functional quadratic form $Q(f) = \langle f, \mathcal{T}f \rangle$, where \mathcal{T} is the centered integral operator associated with kernel k . By the Spectral Theorem, this decomposes as $Q(f) = \sum \lambda_i |\langle f, \phi_i \rangle|^2$. For the test to be *universally consistent*—capable of detecting any non-constant spatial pattern— \mathcal{T} must be strictly positive definite on the subspace orthogonal to the constant function (Theorem 2, Supplementary Note 3).

Standard adjacency-based methods, such as Moran’s I and Hotspot⁵, fail this criterion because the adjacency kernel \mathbf{W} possesses both positive eigenvalues (corresponding to clustering) and negative eigenvalues (corresponding to checkerboard patterns). Consequently, a pattern f projecting onto both positive and negative eigenmodes can suffer from spectral cancellation, yielding $Q(f) \approx 0$ and making the test inconsistent. To rectify this, we utilize a kernel derived from the Conditional Autoregressive (CAR) model¹⁶, $\mathbf{K} = (\mathbf{I} - \rho\tilde{\mathbf{W}})^{-1}$. This transformation maps the eigenvalues μ_i of the normalized adjacency $\tilde{\mathbf{W}}$ to $(1 - \rho\mu_i)^{-1}$. For $\rho \in (0, 1)$, the mapping ensures a strictly positive spectrum, thereby guaranteeing consistency against all functional (mean-dependent) spatial patterns.

2.3 Scalable implementation of Q-tests.

Given a single-gene expression vector \mathbf{x} and spatial coordinates \mathbf{s} (or a predefined kernel matrix \mathbf{K}), we compute the statistic Q_{obs} and its standardized Z-score $Z_{\text{obs}} = (Q_{\text{obs}} - \text{tr}(\mathbf{K})) / \sqrt{2\text{tr}(\mathbf{K}^2)}$ (for cross-kernel comparison). The p -value is derived by approximating the null distribution (a weighted sum of χ^2 variables) via moment matching, using either the Welch-Satterthwaite method, which fits a Gamma distribution using the first two moments, or Liu’s method²⁴, which utilizes four moments for higher accuracy but requires spectral information. Since naive matrix forming ($O(N^2)$) and factorization ($O(N^3)$) are prohibitive for large datasets, we implement two scalable strategies based on spatial geometry.

For arbitrary geometries, we exploit the sparsity of the CAR precision matrix (the Laplacian). Instead of explicit inversion, we compute matrix-vector products \mathbf{Kz} using sparse linear solvers. Trace terms (e.g., $\text{tr}(\mathbf{K}^2)$) are estimated via Hutchinson’s stochastic estimator¹⁸ using random probe vectors, avoiding dense matrix storage entirely. For data collected on regular grids, the kernel matrix is Block-Toeplitz. We compute matrix-vector products as 2D convolutions using the Fast Fourier Transform (FFT), $\mathbf{Kz} = \mathcal{F}^{-1}(\mathcal{F}(\mathbf{k}) \odot \mathcal{F}(\mathbf{z}))$. This reduces complexity to $O(N \log N)$ and yields the exact eigenvalues of \mathbf{K} , enabling the use of the more accurate Liu approximation without additional computational penalty.

2.4 Co-expression analysis using the bivariate R-statistic.

We extend the univariate Q-statistic to the bivariate R-statistic, defined by the bilinear form $R_{xy} = \mathbf{x}^\top \mathbf{Ky}$, to quantify spatial co-variation²¹ between centered, standardized features \mathbf{x} and \mathbf{y} . Geometrically, R_{xy} represents the inner product in the Reproducing Kernel Hilbert Space (RKHS) induced by \mathbf{K} . It generalizes Pearson correlation (recovering it when $\mathbf{K} = \mathbf{I}$) by weighting feature alignment according to spatial proximity. Like the Q-statistic, R_{xy} is sensitive to the spectral properties of \mathbf{K} . Indefinite kernels, such as standard adjacency matrices containing negative eigenvalues, can cause signal cancellation in the RKHS. This may yield $R_{xy} \approx 0$ even for spatially dependent features; in extreme cases, indefiniteness allows a signal to have zero correlation with itself. To ensure consistency, we employ strictly positive definite kernels, such as the CAR kernel.

Under the null hypothesis of spatial independence, R_{xy} is asymptotically normal with mean zero and variance $\text{tr}(\mathbf{K}^2)$, facilitating efficient hypothesis testing via the Central Limit Theorem (CLT). To enable genome-wide analysis, we implement a memory-efficient block-wise computation strategy. We compute the term \mathbf{Ky} in chunks using the scalable methods described previously: implicit sparse solvers for general geometries, and FFT-based convolution for regular grids. For the latter, the operation simplifies to element-wise multiplication in the frequency domain, $\hat{\mathbf{k}} \odot \mathcal{F}(\mathbf{y})$, where $\hat{\mathbf{k}}$ represents the eigenvalues of the Block-Toeplitz kernel.

2.5 Empirical evaluation on spatial and single-cell lineage-tracing data.

To assess test robustness, we conducted a gene-ranking experiment by simulating 100 genes from a negative binomial model (dispersion $\phi = 0.1$; mean expression $\mu \in \{0.1, 0.5\}$, 50 replicates each) with a ground truth spatial pattern corrupted by varying noise levels. Genes were ranked by the Q-statistic per kernel or its associated p -value, computed via CLT for Moran’s I, the Welch approximation for other matrix kernels, or the Liu method for other FFT-based kernels.

For real spatial data, we analyzed a Visium HD mouse small intestine dataset¹⁹ preprocessed by Space Ranger v3.0, comprising 164,800 bins at 16 μm resolution, and 656,788 bins at 8 μm . The dataset was

parsed and formatted using `SpatialData`²⁵ (downloaded from https://s3.embl.de/spatialdata/spatialdata-sandbox/visium_hd_3.0.0_io.zip). Gene expression inputs were generated using the `rasterize_bins` at the specified resolutions; genes with fewer than 10 total transcripts were excluded. We evaluated four kernels under the periodic boundary condition: Gaussian (bandwidth $\sigma = 2.0$), Matérn ($\nu = 1.5, \sigma = 2.0$), Moran's I, and CAR. For the latter two, adjacency was defined by first-order physical neighbors ($k = 4$), with $\rho = 0.9$ for CAR. P -values were computed via CLT for Moran's I and the Liu method for the remaining kernels using the full spectrum. Statistical significance was determined at $\alpha = 0.01$ after Benjamini-Hochberg correction²⁶. For cross-resolution comparisons, outlier and control groups were defined based on Z-score deviation from the identity line. Spatial co-expression analysis was performed on the top 2,000 spatially variable genes identified by the CAR kernel at 8 μm resolution, and R-statistics were computed using the same kernel configurations.

For tumor heritability and plasticity detection, we analyzed a single-cell dataset²³ from a metastatic lung cancer mouse model with lineage resolved experimentally via Cas9-based lineage barcodes. We obtained processed expression data, cell state annotations, and `Cassiopeia`²⁷-reconstructed phylogenetic trees from the original study at <https://zenodo.org/records/5847462#.YrFDKuzMI6A>. Single-cell gene counts were normalized by the median unique molecular identifier (UMI) count across cells and then log-scaled. Neighborhood graphs were constructed from the trees for each tumor individually using a hierarchical weighting scheme: weights of 1.0, 0.5, and 0.25 were assigned to first-, second-, and third-degree siblings (cells sharing immediate to great-grandparent ancestors), respectively. The resulting adjacency matrices were double-normalized to ensure unit degree per cell. For each tumor, we computed Moran's I and CAR- Q ($\rho = 0.9$) for log-normalized gene expression and one-hot encoded cell states present in at least 10 cells. P -values were computed using a CLT null for Moran's I and a Welch null approximation for CAR, with significance determined at $\alpha = 0.05$ after Benjamini-Hochberg correction²⁶. Graph co-expression analysis was restricted to the intersection of significant genes detected by both methods, and R-statistics were computed using the same kernel configurations. Tumors yielding fewer than 10 significant pairs were excluded from the co-expression analysis.

3 Data Availability

This paper analyzes existing, publicly available data without generating new primary data. Processed 10X Visium HD data of a mouse small intestine sample are available in `SpatialData` format via https://s3.embl.de/spatialdata/spatialdata-sandbox/visium_hd_3.0.0_io.zip. Processed single-cell lineage-tracing data of mouse metastatic lung cancer and inferred phylogenetic trees are available via Zenodo (<https://zenodo.org/records/5847462#.YrFDKuzMI6A>).

4 Code Availability

Spatial univariate Q-tests and bivariate R-tests are implemented as part of the `quadsV` Python package, available via GitHub at <https://github.com/JiayuSuPKU/EquivSVT> under BSD-3 License. Code and scripts to reproduce this paper are available via the same repository.

5 Acknowledgements

This work was funded by the National Institutes of Health, National Cancer Institute (grant nos. R35CA253126, U01CA243073, P01CA285250 to R.R.), the Edward P. Evans Center for MDS at Columbia University (to J.S. and R.R.) and the National Science Foundation (grant no. CAREER DBI2146398 to D.A.K.). D.Y. is supported by a Damon Runyon Dale Frey Award, an NCI Transition Career Development Award 1K22CA289207, an NIH Director's New Innovator Award 1DP2OD037078, and a Lung Cancer Research Foundation Leading Edge Award. Any opinions, findings and conclusions or recommendations expressed in this material are those of the authors and do not necessarily reflect the views of the NSF or the NIH.

6 Author Contributions

J.S. conceived the project, implemented Q-tests, conducted theoretical analysis and applications on real data. J.H.F. contributed to the theoretical analysis. H.W. and D.Y. contributed to the lineage-tracing analysis. D.A.K. and R.R. supervised the project. J.S. took lead in writing the article with input from all authors. All authors read and approved the final paper.

7 Competing interests

R.R. is a founder of Genotwin and a member of the Scientific Advisory Board of DiaTech and Flahy. D.Y. is a co-founder of DEM Biopharma. None of these activities are related to the work described in this paper. The other authors declare no competing interests.

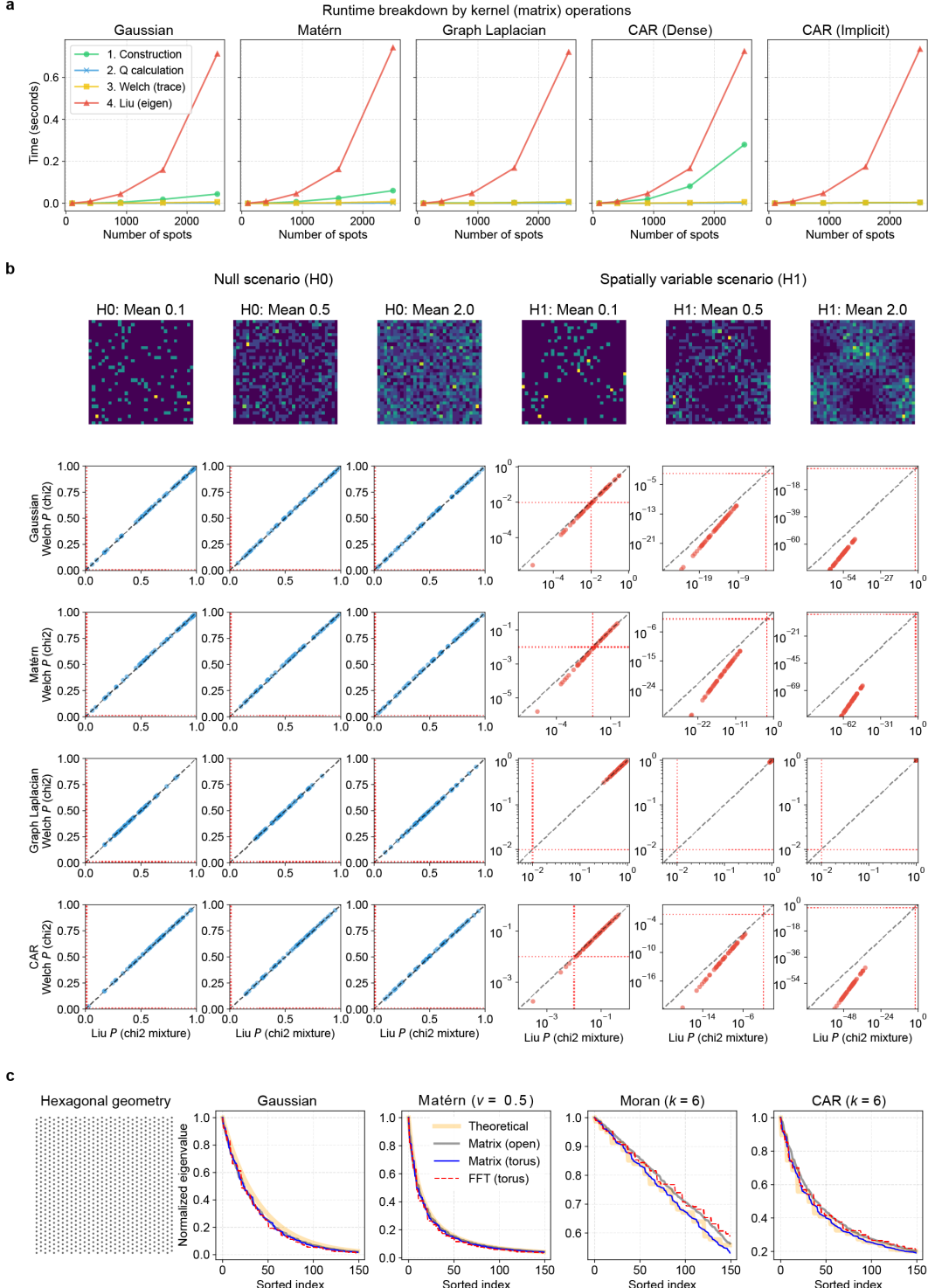


Figure S1: Accuracy and efficiency of spectral approximation. (a) Runtime breakdown of Q-test operations across different kernels. Exact eigen-decomposition for p -value computation (Liu method) represents the primary bottleneck. (b) Comparison of p -values derived from the fast Welch-Satterthwaite approximation (y-axis) and the Liu method (x-axis) under both null and spatially variable scenarios, each with 50 replicates. (c) FFT-based computation of kernel spectra on hexagonal grids. Open: open boundary condition; Torus: periodic boundary condition.

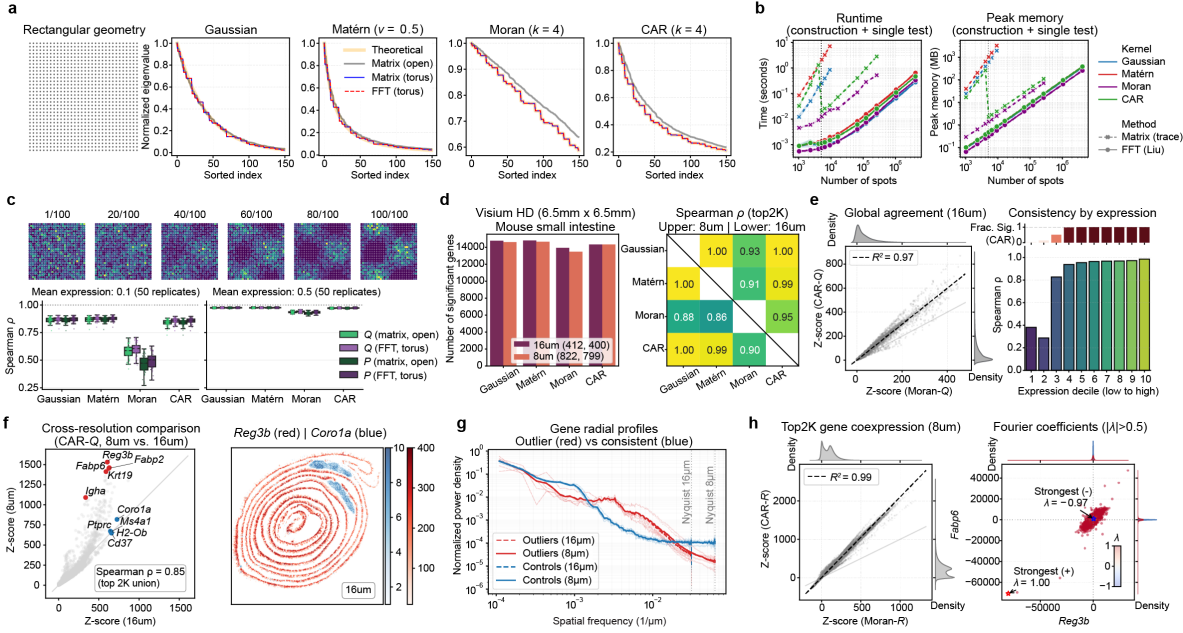


Figure S2: Scaling spatial variability tests to millions of spots. (a) Spectral analysis on rectangular grids. Normalized eigenvalues computed via FFT (torus boundary) closely approximate the exact matrix eigenvalues (open boundary) and theoretical values across all kernels. (b) Runtime and peak memory usage averaged over five replicates, performed on an M1 Macbook Air with 16GB RAM. By design, the CAR kernel switches to implicit mode for $n > 5,000$. (c) Gene-ranking experiment results. A ground truth pattern was corrupted with varying noise levels to generate 100 genes, which were ranked using either the Q-statistic per kernel or its p -value (Welch approximation for matrix kernel, Liu method for FFT kernel). Boxplots show median (center line), interquartile range (box), and $1.5 \times$ interquartile range (whiskers). (d) Test consistency in a Visium HD mouse small intestine sample. Significance was called at $p\text{-adj} < 0.01$. For pairwise comparison, we extracted the top 2,000 genes ranked by each method and computed the Spearman correlation of the Q-statistic on the union gene set. (e) Detailed comparison between CAR and Moran's I. (Left) Scatter plot of Z-scores (Q-statistic normalized by its mean and variance from the null) with a fitted linear regression model. (Right) Per-expression-level test agreement. Top bar shows the fraction of significant SV genes called by CAR ($p\text{-adj} < 0.01$) in each gene group. (f) Cross-resolution analysis ($8 \mu\text{m}$ vs. $16 \mu\text{m}$). Comparison of Z-scores highlights outliers like *Reg3b* (red), which exhibits a “Swiss roll” artifact distinct from immune-cluster signals like *Coro1a* (blue). (g) Radial power density profiles comparing genes with different spatial patterns highlighted in (f). (h) Spatial co-expression analysis using the R-statistic $\mathbf{z}^\top \mathbf{K} \mathbf{y}$. (Left) Scatter plot of Z-scores (R-statistic normalized by its mean and variance from the null) with a fitted linear regression model. (Right) Fourier coefficient analysis of two example genes, confirming that strong negative associations (high-frequency patterns, $\lambda \approx -1$) are rare in biological data, mitigating the theoretical limitations of Moran's R.

References

1. Carstens, J. L. *et al.* Spatial multiplexing and omics. *Nature Reviews Methods Primers* **4**, 54 (2024).
2. Svensson, V., Teichmann, S. A. & Stegle, O. SpatialDE: identification of spatially variable genes. *Nature Methods* **15**, 343–346 (2018).
3. Edsgård, D., Johnsson, P. & Sandberg, R. Identification of spatial expression trends in single-cell gene expression data. *Nature Methods* **15**, 339–342 (2018).
4. Sun, S., Zhu, J. & Zhou, X. Statistical analysis of spatial expression patterns for spatially resolved transcriptomic studies. *Nature Methods* **17**, 193–200 (2020).
5. DeTomaso, D. & Yosef, N. Hotspot identifies informative gene modules across modalities of single-cell genomics. *Cell Systems* **12**, 446–456 (2021).
6. Zhu, J., Sun, S. & Zhou, X. SPARK-X: non-parametric modeling enables scalable and robust detection of spatial expression patterns for large spatial transcriptomic studies. *Genome Biology* **22**, 184 (2021).
7. Chang, Y. *et al.* Graph Fourier transform for spatial omics representation and analyses of complex organs. *Nature Communications* **15**, 7467 (2024).
8. Su, J. *et al.* Mapping isoforms and regulatory mechanisms from spatial transcriptomics data with SPLISOSM. *Nature Biotechnology*, 1–12 (2026).
9. Charitakis, N. *et al.* Disparities in spatially variable gene calling highlight the need for benchmarking spatial transcriptomics methods. *Genome Biology* **24**, 209 (2023).
10. Chen, C., Kim, H. J. & Yang, P. Evaluating spatially variable gene detection methods for spatial transcriptomics data. *Genome Biology* **25**, 18 (2024).
11. Yan, G., Hua, S. H. & Li, J. J. Categorization of 34 computational methods to detect spatially variable genes from spatially resolved transcriptomics data. *Nature Communications* **16**, 1141 (2025).
12. Chen, X. *et al.* Benchmarking algorithms for spatially variable gene identification in spatial transcriptomics. *Bioinformatics* **41**, btaf131 (2025).
13. Moran, P. A. The interpretation of statistical maps. *Journal of the Royal Statistical Society. Series B (Methodological)* **10**, 243–251 (1948).
14. Gretton, A., Bousquet, O., Smola, A. & Schölkopf, B. *Measuring statistical dependence with hilbert-schmidt norms* in *Proceedings of the 16th international conference on Algorithmic Learning Theory* (2005), 63–77.
15. Govek, K. W., Yamajala, V. S. & Camara, P. G. Clustering-independent analysis of genomic data using spectral simplicial theory. *PLoS Computational Biology* **15**, e1007509 (2019).
16. Su, J. *et al.* Smoother: a unified and modular framework for incorporating structural dependency in spatial omics data. *Genome Biology* **24**, 291 (2023).
17. Lindgren, F., Rue, H. & Lindström, J. An explicit link between Gaussian fields and Gaussian Markov random fields: the stochastic partial differential equation approach. *Journal of the Royal Statistical Society Series B: Statistical Methodology* **73**, 423–498 (2011).
18. Hutchinson, M. F. A stochastic estimator of the trace of the influence matrix for Laplacian smoothing splines. *Communications in Statistics-Simulation and Computation* **18**, 1059–1076 (1989).
19. 10x Genomics. *Visium HD Spatial Gene Expression Library, Mouse Small Intestine (FFPE), HD Spatial Gene Expression dataset analyzed using Space Ranger 3.0.0* <https://www.10xgenomics.com/datasets/visium-hd-cytassist-gene-expression-libraries-of-mouse-intestine> (2024).
20. Wartenberg, D. Multivariate spatial correlation: a method for exploratory geographical analysis. *Geographical Analysis* **17**, 263–283 (1985).

21. Li, Z., Wang, T., Liu, P. & Huang, Y. SpatialDM for rapid identification of spatially co-expressed ligand–receptor and revealing cell–cell communication patterns. *Nature Communications* **14**, 3995 (2023).
22. Schiffman, J. S. *et al.* Defining heritability, plasticity, and transition dynamics of cellular phenotypes in somatic evolution. *Nature Genetics* **56**, 2174–2184 (2024).
23. Yang, D. *et al.* Lineage tracing reveals the phylodynamics, plasticity, and paths of tumor evolution. *Cell* **185**, 1905–1923 (2022).
24. Liu, H., Tang, Y. & Zhang, H. H. A new chi-square approximation to the distribution of non-negative definite quadratic forms in non-central normal variables. *Computational Statistics & Data Analysis* **53**, 853–856 (2009).
25. Marconato, L. *et al.* SpatialData: an open and universal data framework for spatial omics. *Nature Methods* **22**, 58–62 (2025).
26. Benjamini, Y. & Hochberg, Y. Controlling the false discovery rate: a practical and powerful approach to multiple testing. *Journal of the Royal Statistical Society: Series B (Methodological)* **57**, 289–300 (1995).
27. Jones, M. G. *et al.* Inference of single-cell phylogenies from lineage tracing data using Cassiopeia. *Genome Biology* **21**, 92 (2020).

Supplementary Note 1 Clarification on kernel terminology

The term “kernel” is notoriously overloaded in computational sciences, carrying distinct definitions across statistics, functional analysis, and machine learning. In this work, we draw upon concepts from these varied fields. To facilitate understanding for readers from diverse backgrounds, we provide this note to clarify our notation and the specific mathematical objects to which we refer.

1.1 The Kernel Function and Kernel Matrix

In its most fundamental form, a **kernel function** $k(s, s')$ is a bivariate function mapping pairs of inputs from a space \mathcal{S} (e.g., spatial locations) to a real number. We assume the kernel is symmetric, such that $k(s, s') = k(s', s)$. The **kernel matrix**, denoted as $\mathbf{K} \in \mathbb{R}^{n \times n}$, is the discrete evaluation of this function on a finite set of n locations $\{s_1, \dots, s_n\}$, where $\mathbf{K}_{ij} = k(s_i, s_j)$.

In machine learning contexts (e.g., Gaussian Processes), kernels are typically required to be positive semi-definite (PSD). However, in the statistical theory of U-statistics and V-statistics, which underpins parts of this work, the kernel function k *need not* be PSD. In that context, it serves primarily as a symmetric weighting function quantifying the relationship between s and s' .

1.2 The Kernel Operator and its spectrum

The kernel matrix \mathbf{K} can be viewed as a discrete approximation of a continuous linear operator called the **kernel operator** $\mathcal{K} : L^2(\mathcal{S}) \rightarrow L^2(\mathcal{S})$, which is induced by k via the integral

$$(\mathcal{K}f)(s) = \int_{\mathcal{S}} k(s, s') f(s') ds'.$$

As an operator, the kernel matrix \mathbf{K} acts on a vector $\mathbf{x} \in \mathbb{R}^n$ to produce another vector $\mathbf{Kx} \in \mathbb{R}^n$. Similarly, the kernel operator \mathcal{K} acts on a function f to produce another function $\mathcal{K}f$. Here, the finite observation vector $\mathbf{x} = f(\mathbf{s}) = \{f(s_1), \dots, f(s_n)\}$ represents the function f evaluated at the sample points. If the sampled spatial locations s_i are drawn uniformly from the metric space \mathcal{S} , the matrix-vector product converges to the integral operation $n \rightarrow \infty$.

The **kernel spectrum** refers to the eigendecomposition of the kernel operator or matrix:

- (Continuous) The eigenvalues λ_j and eigenfunctions ϕ_j of \mathcal{K} satisfy $\int k(s, s') \phi_j(s') ds' = \lambda_j \phi_j(s)$.
- (Discrete) The eigenvalues $\hat{\lambda}_j$ and eigenvectors \mathbf{v}_j of \mathbf{K} satisfy $\mathbf{Kv}_j = \hat{\lambda}_j \mathbf{v}_j$.

Under appropriate regularity conditions, the discrete eigenvalues and eigenvectors converge to their continuous counterparts. Specifically, $\frac{1}{n} \hat{\lambda}_j \rightarrow \lambda_j$, and the eigenvectors \mathbf{v}_j converge to the eigenfunctions ϕ_j evaluated at the sampled spatial locations.

Remark: Not all limits of kernel matrices result in an *global* integral kernel operator defined across \mathcal{S} . A prime example is the Graph Laplacian. Consider a kernel defined by proximity $\mathbf{W}_{ij} = \mathbb{I}(\|s_i - s_j\| < r)$ where r is a given distance cutoff. The nature of the limit operator depends entirely on the behavior of the radius r relative to the sample size n .

- If r remains fixed as $n \rightarrow \infty$, the discrete matrix operation converges to a bounded, linear integral operator \mathcal{K}_r . For a function $f \in L^2(\mathcal{S})$, this operator averages values within a fixed neighborhood

$$(\mathcal{K}_r f)(x) = \int_{B_r(x) := \|x - y\| < r} f(y) dy,$$

producing smoothed results semi-globally depending on the size of r .

- If $r \rightarrow 0$ as $n \rightarrow \infty$ (at a sufficiently slow rate to maintain connectivity), the operator localizes. The normalized Graph Laplacian $\mathbf{L}_{rw} = \mathbf{I} - \mathbf{D}^{-1} \mathbf{W}$ converges point-wise to the Laplace-Beltrami operator Δ ,

$$\lim_{r \rightarrow 0} \frac{1}{r^2} \left(f(x) - \frac{\int_{B_r(x)} f(y) dy}{\text{Vol}(B_r(x))} \right) = -C_d \Delta f(x),$$

where C_d is a dimension-dependent constant. Here, the limit is not an integral operator, but the second-order *local* differential operator $\Delta f = \sum_i \partial^2 f / \partial x_i^2$.

While Δ is not an integral operator, spectral theory still applies. The Spectral Theorem requires only that the operator be compact and self-adjoint (or have a compact resolvent), allowing us to analyze the spectrum of the Laplacian just as we do for integral kernel operators.

1.3 Reproducing Kernel Hilbert Space (RKHS)

When a kernel function k is symmetric and PSD, it uniquely determines a function space known as a **Reproducing Kernel Hilbert Space (RKHS)**, denoted by \mathcal{H}_k . An RKHS can be formulated using many equivalent definitions. One standard way is as a Hilbert space of functions where the evaluation functional $\delta_x : f \mapsto f(x)$ is bounded for all $x \in \mathcal{X}$. By the Riesz Representation Theorem, the boundedness implies the existence of a representer $k(\cdot, x) \in \mathcal{H}_k$ satisfying the *reproducing property*

$$f(x) = \langle f, k(\cdot, x) \rangle_{\mathcal{H}_k}, \quad \forall f \in \mathcal{H}_k, \forall x \in \mathcal{X}.$$

This property allows us to analyze complex, potentially infinite-dimensional functions $f \in \mathcal{H}_k$ implicitly via the inner product and evaluations of the kernel on finite data.

Furthermore, if the domain \mathcal{X} is a compact metric space and k is continuous, Mercer's Theorem guarantees that k admits a spectral decomposition in terms of the eigenfunctions of its associated integral kernel operator \mathcal{K} . Specifically,

$$k(x, x') = \sum_{j=1}^{\infty} \lambda_j \phi_j(x) \phi_j(x'),$$

where $\{\lambda_j\}_{j=1}^{\infty}$ are non-negative eigenvalues and $\{\phi_j\}_{j=1}^{\infty}$ form an orthonormal basis of $L^2(\mathcal{X})$. This establishes that any feature map $\Phi : \mathcal{X} \rightarrow \mathcal{H}_k$ essentially maps data into a high-dimensional Euclidean space defined by these eigenfunctions.

Another central concept in kernel hypothesis testing is the **kernel mean embedding**. We can represent a probability distribution \mathbb{P} over \mathcal{X} as an element $\mu_{\mathbb{P}} \in \mathcal{H}_k$, defined such that $\mathbb{E}_{X \sim \mathbb{P}}[f(X)] = \langle f, \mu_{\mathbb{P}} \rangle_{\mathcal{H}_k}$. Explicitly, this embedding is the expectation of the feature map

$$\mu_{\mathbb{P}} = \mathbb{E}_{X \sim \mathbb{P}}[k(\cdot, X)].$$

Given a finite sample $\{x_i\}_{i=1}^n$, we estimate this embedding empirically as $\hat{\mu}_{\mathbb{P}} = \frac{1}{n} \sum_{i=1}^n k(\cdot, x_i)$. As will be discussed in later sections, kernel dependence measures (such as the Hilbert-Schmidt Independence Criterion) operate by quantifying the distance between the mean embedding of the joint distribution and the product of the marginal embeddings within the RKHS. It is also connected to Mutual Information via kernel density estimators (Supplementary Note 2.7.1).

1.4 Kernels in Convolutional Neural Networks (CNNs)

In image processing, a “kernel” typically refers to a discrete convolution filter, \mathbf{A} , consisting of learnable weights of size $k \times k$. This filter slides across an input image \mathbf{X} of size $n \times n$ to extract local features. Mathematically, the operation can be expressed as a matrix-vector product $\mathbf{K}_{\text{conv}} \cdot \text{vec}(\mathbf{X})$, where $\mathbf{K}_{\text{conv}} \in \mathbb{R}^{n^2 \times n^2}$ is a doubly block Toeplitz matrix generated by \mathbf{A} . Although \mathbf{K}_{conv} is rarely constructed explicitly due to its size, its spectrum is fully determined by the filter \mathbf{A} . Under periodic boundary conditions (where \mathbf{K}_{conv} becomes block circulant), its eigenvalues correspond to the 2D Fourier transform coefficients of the zero-padded filter $\tilde{\mathbf{A}}$ of size $n \times n$,

$$\text{eig}(\mathbf{K}_{\text{conv}}) = \mathcal{F}(\tilde{\mathbf{A}}).$$

This connection allows us to analyze CNN filters using the same spectral tools applied to other pattern detection methods, with two key distinctions. First, \mathbf{K}_{conv} is symmetric only if \mathbf{A} is point symmetric (i.e., $A[i, j] = A[-i, -j]$). Second, for \mathbf{K}_{conv} to be PSD, the small filter must satisfy $\mathbf{A} = \mathbf{B} * \text{flip}(\mathbf{B})$, the convolutional equivalent of the Cholesky decomposition $\mathbf{A} = \mathbf{B}\mathbf{B}^{\top}$. When these conditions hold, a learned CNN kernel defines a proper statistic for global (image-level) pattern detection by the quadratic form $Q = \text{vec}(\mathbf{X})^{\top} \mathbf{K}_{\text{conv}} \text{vec}(\mathbf{X})$.

Supplementary Note 2 Equivalence between spatial variability tests

In this section, we demonstrate that virtually all spatial variability tests—despite originating from distinct statistical traditions such as autocorrelation, mixed models, and kernel methods—can be unified under a general quadratic form test statistic Q_n . We then prove a common limitation for tests based on the Q-statistic: they are consistent only with respect to mean-shift dependencies (Theorem 1).

2.1 Problem formulation

We begin by formalizing spatial variability through the lens of statistical dependency.

Definition 2.1 (Spatial Variability). *Let X be a random variable representing a feature of interest (e.g., gene expression) and S be a random variable representing spatial coordinates. We say X exhibits spatial variability if X and S are statistically dependent. That is, the joint density does not factorize into the product of marginals,*

$$f_{X,S}(x, s) \neq f_X(x)f_S(s).$$

In experimental settings, we observe a dataset with n pairs $\{(x_i, s_i)\}_{i=1}^n$. Testing for spatial variability is equivalent to testing whether the distribution of X given S varies across some physical space \mathcal{S} . We conceptualize the data generation process as first sampling a location s from $\mathcal{S} \subseteq \mathbb{R}^3$, followed by drawing x from the conditional distribution $X|S = s$. Independence thus implies that the conditional distribution $X|S$ is invariant across \mathcal{S} (i.e., $P(X|S = s) = P(X)$ for all s), yielding the following result:

Proposition 2.1. *If X and S are statistically independent, then the observed values $\{x_i\}_{i=1}^n$ are independent and identically distributed (i.i.d.) samples from the marginal distribution $f_X(x)$.*

Remark: Proposition 2.1 allows us to derive the general null distribution for spatial statistics, which *does not* depend on the form of dependence or patterns under the alternative. However, the converse does not hold; marginal i.i.d. properties do not guarantee that $X|S$ is independent. Furthermore, for spatial omics data, we typically only observe a single realization x_i at each unique location s_i , precluding direct estimation of the conditional density $X|S = s_i$.

Let $\mathbf{s} = \{s_1, \dots, s_n\} \in \mathcal{S}^n$ be the spatial coordinates of n samples, and $\mathbf{x} = \{x_1, \dots, x_n\} \in \mathcal{X}^n$ be the vector of observations (e.g., the expression of a single gene) at the n sampled locations. While each $x_i \in \mathcal{X}$ can be multivariate (e.g., isoform usage ratios within a gene)¹, we assume without loss of generality that X takes a scalar value and $\mathcal{X} \subseteq \mathbb{R}$. Under the null hypothesis that \mathbf{x} contains i.i.d. entries, $\mathbb{E}[\mathbf{x}] = \mu\mathbf{1}$ and $\text{Var}(\mathbf{x}) = \sigma^2\mathbf{I}$. We also assume access to μ and σ^2 (or their sample estimators), such that we can compute the standardized data $\mathbf{z} = \frac{\mathbf{x} - \mu}{\sigma}$. Under the null, $\mathbb{E}[\mathbf{z}] = \mathbf{0}$ and $\text{Var}(\mathbf{z}) = \mathbf{I}$.

Definition 2.2 (Q-statistic). *Given standardized data $\mathbf{z} \in \mathbb{R}^n$ and a symmetric kernel matrix $\mathbf{K} \in \mathbb{R}^{n \times n}$, we define the Q-statistic as the quadratic form*

$$Q_n = \mathbf{z}^\top \mathbf{K} \mathbf{z}.$$

For the remainder of this note, we will demonstrate how seemingly different spatially variable gene (SVG) detection methods all reduce to this same quadratic form. Table 1 summarizes some of the results. Even though different SVG tests were developed for distinct alternative hypotheses, the equivalence we established here will allow us to systematically compare them, examine test consistency under Definition 2.1 and improve test design (Supplementary Note 3).

2.2 Asymptotic behavior of the quadratic form Q-statistic

The quadratic form naturally occurs in various statistical problems, and its asymptotical behavior has been studied extensively. Under the null hypothesis of no spatial variability, the mean and variance of Q_n are given by,

$$\mathbb{E}[Q_n] = \mathbb{E}[\text{tr}(\mathbf{z}^\top \mathbf{K} \mathbf{z})] = \text{tr}(\mathbf{K} \mathbb{E}[\mathbf{z} \mathbf{z}^\top]) = \text{tr}(\mathbf{K}) \quad (1)$$

$$\text{Var}(Q_n) = \sum_i \sum_j \sum_k \sum_l K_{ij} K_{kl} \mathbb{E}[z_i z_j z_k z_l] - (\text{tr}(\mathbf{K}))^2 = (\mu_4 - 3) \sum_{i=1}^n K_{ii}^2 + 2\text{tr}(\mathbf{K}^2),$$

Table 1: Equivalence of spatial variability tests to $Q_n = \mathbf{z}^\top \mathbf{K} \mathbf{z}$ under the null

Method/model ¹	Alternative hypothesis ²	Effective \mathbf{K}
Moran's I and other adjacency-based	spatial autocorrelation $\neq 0$	\mathbf{W} (spatial weights)
Linear fixed effect	$\beta \neq \mathbf{0}$	$\mathbf{L}(\mathbf{L}^\top \mathbf{L})^{-1} \mathbf{L}^\top$ (projection)
Linear random effect (LMM)	$\sigma_s^2 > 0$ (variance comp.)	\mathbf{K}_{cov} (spatial covariance)
Generalized fixed effect (GLM) ³	$\beta \neq \mathbf{0}$	$\mathbf{L}(\mathbf{L}^\top \mathbf{L})^{-1} \mathbf{L}^\top$
Generalized random effect (GLMM) ³	$\sigma_s^2 > 0$	\mathbf{K}_{cov}
HSIC (linear data kernel)	$\mathbb{E}[X S] \neq \mathbb{E}[X]$	\mathbf{K} (spatial kernel)
χ^2 -divergence (linear data kernel)	$\mathbb{E}[X S] \neq \mathbb{E}[X]$	$k(\cdot, \cdot)$ (density estimator)

¹Due to space limits, references to representative methods are provided in the corresponding sections.

²None of these alternatives cover all spatial variability forms defined in Definition 2.1.

³For non-Gaussian data, \mathbf{z} (and thus Q_n) is scaled by a global factor depending on the mean of \mathbf{x} .

where $\mu_4 = \mathbb{E}[z_i^4]$ is the kurtosis of the distribution of Z . If the data is Gaussian, $\mu_4 = 3$, simplifying the variance to $\text{Var}(Q_n) = 2\text{tr}(\mathbf{K}^2)$. Note that the size of \mathbf{K} and thus its trace will vary based on sample size n . For simplicity, we omit the subscript index n in \mathbf{K}_n and Q_n unless needed for clarity. In hypothesis testing, we assume \mathbf{K} is generated from spatial coordinates via a symmetric function, such that $\mathbf{K}_{ij} = k(s_i, s_j)$. Defining $y_i = (z_i, s_i)$, we can rewrite the statistic as,

$$Q_n = \sum_{i=1}^n \sum_{j=1}^n z_i z_j k(s_i, s_j) =: \sum_{i=1}^n \sum_{j=1}^n H(y_i, y_j).$$

Here, $H(y_i, y_j) = z_i z_j k(s_i, s_j) = z_j z_i k(s_j, s_i) = H(y_j, y_i)$ is a symmetric kernel function defined over the joint data y . That is, $n^{-2}Q_n$ corresponds to a degenerate V-statistic^{2,3} whose asymptotic distribution converges to a weighted sum of independent chi-square variables,

$$\frac{1}{n} Q_n \xrightarrow{d} \sum_k \lambda_k Z_k^2, \quad (2)$$

where $\{\lambda_k\}$ are the eigenvalues of the integral operator $\mathcal{H} : (\mathcal{H}f)(y) = \int H(y, y')f(y')dy'$. Since \mathcal{H} is the tensor product of $\mathcal{K} : (\mathcal{K}f)(s) = \int k(s, s')f(s')ds'$ and the linear kernel integral operator $(\mathcal{L}f)(z) = \int z z' f(z')dz'$ (with eigenvalues zero and $1 = \int z^2 dz$), it shares the same eigenvalues with \mathcal{K} . For finite samples, $\{\lambda_k\}_{k=1}^n$ are the spectrum of the kernel matrix \mathbf{K} , and the null distribution is commonly approximated using the Welch-Satterthwaite method (matching moments to a single scaled χ^2 distribution). We refer to the testing procedure using the statistic Q and the null moments in Eq. (1) (or other null approximations) as a **Q-test**.

What Eq. (1) does not tell us, however, is the behavior of Q under the alternative hypothesis that X is spatially variable. As we will see in later sections, the consistency (i.e., whether the test almost always rejects the null under *any* alternative hypothesis as sample size increases) and statistical power of Q-tests depend critically on the spectral design of \mathbf{K} .

2.3 Moran's I as a Q-test

Moran's I, initially introduced by Moran [4] and popularized by Cliff & Ord [5], remains the canonical and arguably most important measure of spatial autocorrelation. Given observations $\mathbf{z} \in \mathbb{R}^n$, it is defined as

$$I = \frac{n}{\sum_{i,j} w_{ij}} \frac{\mathbf{z}^\top \mathbf{H} \mathbf{W} \mathbf{H} \mathbf{z}}{\mathbf{z}^\top \mathbf{H} \mathbf{z}},$$

where \mathbf{W} is the spatial weight matrix and $\mathbf{H} = \mathbf{I} - \frac{1}{n} \mathbf{1} \mathbf{1}^\top$ is the centering matrix. For standardized data, $\mathbf{z}^\top \mathbf{H} \mathbf{z} \approx n$ and $\mathbf{H} \mathbf{z} = \mathbf{z}$. Thus, we can reformulate Moran's I as a quadratic form governed by the weight matrix

$$I = \frac{1}{\sum_{i,j} w_{ij}} \mathbf{z}^\top \mathbf{W} \mathbf{z} \propto Q_{\text{Moran}} := \mathbf{z}^\top \mathbf{W} \mathbf{z}. \quad (3)$$

Here, we assume \mathbf{W} is symmetric (e.g., from mutual k -nearest-neighbor graphs). Moran's I can also be defined for asymmetric \mathbf{W}' , which is technically not a kernel matrix by Supplementary Note 1. In practice, it is common to symmetrize the weight matrix via $\mathbf{W} = \frac{1}{2}(\mathbf{W}' + \mathbf{W}'^\top)$ to improve robustness to outliers and density variations. Many variants of Moran's I have been developed for SVG detection, such as **Hotspot**⁶ and **MERINGUE**⁷. These methods typically differ in their strategies for constructing \mathbf{W} . However, as long as the kernel spectrum remains indefinite (containing both positive and negative eigenvalues), the theoretical limitations of Moran's I apply to all these methods, as will be demonstrated in Supplementary Note 3.

Beyond its role as a descriptive statistic, Moran's I is intrinsically linked to parametric inference. Burridge [8] first showed that the test based on Moran's I is equivalent to the score test for a Simultaneous Autoregressive (SAR) spatial random process model. Below, we extend this finding and show that this quadratic form also emerges naturally from mixed models with more general covariance structures.

2.4 Linear Model tests as Q-tests

2.4.1 Linear fixed effects models

Consider a linear regression framework where spatial dependence is captured through a set of fixed spatial covariates. Let $\mathbf{L} \in \mathbb{R}^{n \times d}$ denote a design matrix constructed from a spatial feature map $\phi : \mathcal{S} \rightarrow \mathbb{R}^d$, such that the i -th row corresponds to $\mathbf{L}_i = \phi(\mathbf{s}_i)^\top$. These features may represent basis functions (e.g., splines), geometric descriptors (e.g., distance to landmarks), or, in the context of cell-type-specific testing, estimated cellular abundance maps. The model is defined as

$$\mathbf{z} = \mathbf{L}\boldsymbol{\beta} + \boldsymbol{\epsilon}, \quad \boldsymbol{\epsilon} \sim \mathcal{N}(\mathbf{0}, \sigma^2 \mathbf{I}).$$

σ is a nuisance parameter typically estimated separately via maximum likelihood estimation (MLE) under the null (for standardized data $\hat{\sigma} \approx 1$). To derive the test statistic, we utilize the score test, which requires the gradient of the log-likelihood and the Fisher information matrix evaluated at $\boldsymbol{\beta} = \mathbf{0}$. The log-likelihood of the model is $\ell(\boldsymbol{\beta}) \propto -\frac{1}{2\sigma^2}(\mathbf{z} - \mathbf{L}\boldsymbol{\beta})^\top(\mathbf{z} - \mathbf{L}\boldsymbol{\beta})$. The score vector (gradient) with respect to $\boldsymbol{\beta}$, evaluated at the null, is

$$\mathbf{U}(\mathbf{0}) = \frac{\partial \ell}{\partial \boldsymbol{\beta}} \Big|_{\boldsymbol{\beta}=\mathbf{0}} = \frac{1}{\sigma^2} \mathbf{L}^\top \mathbf{z}.$$

The expected Fisher information matrix for $\boldsymbol{\beta}$ is

$$\mathcal{I}(\mathbf{0}) = \mathbb{E} \left[-\frac{\partial^2 \ell}{\partial \boldsymbol{\beta} \partial \boldsymbol{\beta}^\top} \right] = \frac{1}{\sigma^2} \mathbf{L}^\top \mathbf{L}.$$

The score statistic is given by the quadratic form $S_{\text{fixed}} = \mathbf{U}(\mathbf{0})^\top [\mathcal{I}(\mathbf{0})]^{-1} \mathbf{U}(\mathbf{0})$. Substituting the terms above and simplifying (assuming $\sigma^2 \approx 1$ for standardized data), we obtain

$$S_{\text{fixed}} = \mathbf{z}^\top \mathbf{L} (\mathbf{L}^\top \mathbf{L})^{-1} \mathbf{L}^\top \mathbf{z} =: \mathbf{z}^\top \mathbf{K}_{\text{proj}} \mathbf{z}. \quad (4)$$

Here, \mathbf{K}_{proj} is the orthogonal projection matrix (hat matrix) onto the column space of \mathbf{L} . The score statistic follows χ_d^2 under the null, corresponding precisely to a Q-test with $\mathbf{K} = \mathbf{K}_{\text{proj}}$ (which has d eigenvalues of 1). Geometrically, this statistic measures the magnitude of the signal that can be explained by the spatial basis \mathbf{L} . In the context of RKHS theory, if we define a linear kernel $\mathbf{K}_{\text{lin}} = \mathbf{L}\mathbf{L}^\top$, the matrix \mathbf{K}_{proj} can be interpreted as a “whitened” kernel matrix, where directions in the feature space are normalized to have unit variance.

The linear fixed effect regression model is most popular in cell-type-specific spatial variability testing, which we will discuss in depth in Section 2.8.

2.4.2 Linear random effects models (LMM)

Following the pioneering work of **SpatialDE**⁹, we consider a Linear Mixed Model (LMM) where spatial structure is modeled as a random effect rather than a fixed covariate,

$$\mathbf{z} \sim \mathcal{N}(\mathbf{0}, \sigma^2 \mathbf{I} + \theta \mathbf{K}_{\text{cov}}). \quad (5)$$

Here, \mathbf{K}_{cov} is a fixed, positive-definite spatial covariance matrix (e.g., a Gaussian kernel based on spatial locations), σ^2 is the noise variance (nuisance parameter, $\hat{\sigma}^2 \approx 1$ for standardized data), and $\theta \geq 0$ is the variance component governing spatial variability.

To test for spatial structure ($H_0 : \theta = 0$ vs. $H_1 : \theta > 0$), we derive the score statistic. The log-likelihood is $\ell(\theta) \propto -\frac{1}{2} \ln |\Sigma_\theta| - \frac{1}{2} \mathbf{z}^\top \Sigma_\theta^{-1} \mathbf{z}$. Using the derivative of the covariance matrix $\frac{\partial \Sigma_\theta}{\partial \theta} = \mathbf{K}_{\text{cov}}$ and the matrix identity $\frac{\partial \Sigma^{-1}}{\partial \theta} = -\Sigma^{-1} \frac{\partial \Sigma}{\partial \theta} \Sigma^{-1}$, the score evaluated at the null ($\theta = 0$, $\Sigma_0 = \sigma^2 \mathbf{I}$) is

$$U(0) = -\frac{1}{2} \text{tr}(\Sigma_0^{-1} \mathbf{K}_{\text{cov}}) + \frac{1}{2} \mathbf{z}^\top \Sigma_0^{-1} \mathbf{K}_{\text{cov}} \Sigma_0^{-1} \mathbf{z} = \frac{1}{2\sigma^4} (\mathbf{z}^\top \mathbf{K}_{\text{cov}} \mathbf{z} - \sigma^2 \text{tr}(\mathbf{K}_{\text{cov}})).$$

The Fisher information at the null is $\mathcal{I}(0) = \frac{1}{2} \text{tr}(\Sigma_0^{-1} \mathbf{K}_{\text{cov}} \Sigma_0^{-1} \mathbf{K}_{\text{cov}}) = \frac{1}{2\sigma^4} \text{tr}(\mathbf{K}_{\text{cov}}^2)$. The standard score statistic $S = U(0)^2 / \mathcal{I}(0)$, assuming standardized data ($\sigma^2 \approx 1$), becomes

$$S_{\text{LMM}} = \frac{1}{2\text{tr}(\mathbf{K}_{\text{cov}}^2)} (\mathbf{z}^\top \mathbf{K}_{\text{cov}} \mathbf{z} - \text{tr}(\mathbf{K}_{\text{cov}}))^2, \quad (6)$$

which is equivalent to a Q-test using the spatial covariance matrix as the kernel. The expression $Q_{\text{LMM}} = \mathbf{z}^\top \mathbf{K}_{\text{cov}} \mathbf{z}$ provides a natural interpretation of the Q-statistic. Under a Gaussian random field prior $\mathbf{z} \sim \mathcal{N}(\mathbf{0}, \mathbf{K}_{\text{cov}})$, the negative log-likelihood is proportional to $\mathbf{z}^\top \mathbf{K}_{\text{cov}}^{-1} \mathbf{z}$. A large Q implies that \mathbf{z} aligns with the dominant modes of \mathbf{K}_{cov} , effectively minimizing the negative log-likelihood and indicating that the signal is highly consistent with the spatial prior.

Remark: `SpatialDE`⁹ uses a likelihood ratio (LR) test with χ_1^2 null for hypothesis testing, which is asymptotically equivalent to Eq. (6) under the null and local alternatives (e.g., $\theta \approx 0$). A theoretical nuance arises because the null hypothesis $\theta = 0$ lies on the boundary of the parameter space ($\theta \geq 0$). Consequently, the asymptotic distribution of the LR statistic is not the standard χ_1^2 , but rather a mixture $0.5\chi_0^2 + 0.5\chi_1^2$, a result established by Chernoff [10]. Furthermore, LMM (and its generalized version) is also called Gaussian Process (GP) regression, and more scalable implementations have since been developed, such as `SOMDE`¹¹ and `nnSVG`¹², both of which also use LR for hypothesis testing.

Finally, we note that different model parameterizations of the covariance in Eq. (5) can yield identical test statistics. This is best illustrated by the SAR model studied by Burridge [8],

$$\mathbf{z} = \rho \mathbf{W} \mathbf{z} + \epsilon \implies \mathbf{z} \sim \mathcal{N}(\mathbf{0}, \sigma^2 [(\mathbf{I} - \rho \mathbf{W})^\top (\mathbf{I} - \rho \mathbf{W})]^{-1}),$$

where $\rho \in [0, 1]$ is called the spatial autoregressive parameter and \mathbf{W} is a row-normalized adjacency matrix with zero diagonal. Testing for spatial dependence ($H_0 : \rho = 0$) involves the derivative of the log-likelihood with respect to ρ . At $\rho = 0$, the derivative of the log-determinant term vanishes (as $\text{tr}(\mathbf{W}) = 0$), and the derivative of the quadratic term is determined by $\frac{\partial}{\partial \rho} [(\mathbf{I} - \rho \mathbf{W})^\top (\mathbf{I} - \rho \mathbf{W})] |_{\rho=0} = -(\mathbf{W} + \mathbf{W}^\top)$. Thus, the score is proportional to $\mathbf{z}^\top (\mathbf{W} + \mathbf{W}^\top) \mathbf{z} = 2\mathbf{z}^\top \mathbf{W} \mathbf{z}$, recovering the numerator of Moran's I. This result shows that Moran's I is the score statistic for the SAR model, equivalent to an LMM test with an improper kernel $\mathbf{K}_{\text{cov}} = \mathbf{W}$.

2.5 Generalized Linear Model tests as Q-tests

In domains such as single-cell and spatial transcriptomics, data are often non-Gaussian. It is therefore standard practice to employ Generalized Linear Models (GLMs) under the assumption that explicit parametric modeling captures the data-generating process more accurately, thereby enhancing statistical power. For the specific task of spatial variability testing, our following analysis reveals that the power gain is primarily attributable to a gene-specific scaling of the Q-statistic. Compared to Gaussian-based Q-tests, this scaling implicitly prioritizes genes with higher expression levels.

2.5.1 Generalized linear models (GLMs)

Consider a GLM where the response vector \mathbf{x} (of size n) follows a distribution from the exponential family (e.g., Poisson as used in `C-SIDE`¹³). We assume a canonical link function $g(\cdot)$, relating the mean $\boldsymbol{\mu} = \mathbb{E}[\mathbf{x}]$ to the linear predictor by

$$\boldsymbol{\eta} = g(\boldsymbol{\mu}) = \mathbf{b} \mathbf{1} + \mathbf{L} \boldsymbol{\beta},$$

where b is the intercept and \mathbf{L} is the matrix of fixed spatial effects. We test the null hypothesis of no spatial effect $H_0 : \boldsymbol{\beta} = \mathbf{0}$. Under H_0 , the MLE mean estimator is constant, $\hat{\mu}_0 = g^{-1}(\hat{b}) = \bar{\mathbf{x}}$. The score vector with respect to $\boldsymbol{\beta}$ is thus defined as

$$U(\boldsymbol{\beta})|_{\boldsymbol{\beta}=0} = \mathbf{L}^\top \mathbf{W}_0(\boldsymbol{\eta} - \hat{\boldsymbol{\eta}}) = \mathbf{L}^\top \mathbf{W}_0(\mathbf{x} - \hat{\mu}_0).$$

Here, $\mathbf{W} = \text{diag}\left(\frac{1}{V(\mu_i)[g'(\mu_i)]^2}\right)$ is the GLM working weights matrix where $V(\cdot)$ is the variance function. Under the null, $\mathbf{W}_0 = w_0 \mathbf{I}$. The resulting score statistic is given by

$$S_{\text{GLM}} = (\mathbf{x} - \hat{\mu}_0)^\top \mathbf{W}_0 \mathbf{L} (\mathbf{L}^\top \mathbf{W}_0 \mathbf{L})^{-1} \mathbf{L}^\top \mathbf{W}_0 (\mathbf{x} - \hat{\mu}_0),$$

which follows χ_d^2 under the null hypothesis. To elucidate the relationship with linear models, we defined the standardized residuals $\mathbf{z}_0 = \mathbf{W}_0^{1/2}(\mathbf{x} - \hat{\mu}_0) \equiv \frac{\mathbf{x} - \mu_0}{v_0}$. Here, $v_0 = w_0^{-1/2} := \sqrt{\text{Var}(\hat{\mu}_0)} g'(\hat{\mu}_0)$ can be understood as the standard deviation of the working variable under the null. Substituting this into the score equation yields

$$S_{\text{GLM}} = \mathbf{z}_0^\top \mathbf{K}_{\text{proj}} \mathbf{z}_0 = \frac{\hat{\sigma}^2}{v_0^2} S_{\text{fixed}}, \quad (7)$$

where $\mathbf{K}_{\text{proj}} = \mathbf{L}(\mathbf{L}^\top \mathbf{L})^{-1} \mathbf{L}^\top$ is the projection matrix associated with the spatial features, and S_{fixed} is the statistic derived from a standard linear model.

Eq. (7) highlights that a GLM-based Q-test on raw counts is structurally identical to a linear test on standardized data, up to a scalar factor $\frac{\hat{\sigma}^2}{v_0^2}$. If the parametric assumptions hold, the sample variance $\hat{\sigma}^2$ converges to the model-implied variance. For common distributions we have

- **Gaussian:** $v_0^2 = \hat{\sigma}^2$, yielding a ratio of 1. The GLM recovers the standard linear test.
- **Poisson:** $v_0^2 = \hat{\mu}_0(1/\hat{\mu}_0)^2 = \hat{\mu}_0^{-1}$. The ratio converges to $\hat{\mu}_0/\hat{\mu}_0^{-1} = \hat{\mu}_0^2$ for large sample sizes.
- **Negative Binomial:** With dispersion r , $v_0^2 = 1/\text{Var}(\hat{\mu}_0) = (\hat{\mu}_0 + \hat{\mu}_0^2/r)^{-1}$. The ratio converges to $(\hat{\mu}_0 + \hat{\mu}_0^2/r)^2$ for large sample sizes.

In essence, GLM-based Q-tests “inflate” the test statistic by gene expression levels while maintaining the same null structure as linear regression models. Genes with higher expression exhibit lower “effective variance” (v_0^2), resulting in a stronger statistical signal. This prioritization procedure is analogous to workflows in highly variable gene (HVG) identification for single-cell analysis, where data is often standardized using only the technical (mean-dependent) variance component, deliberately preserving biological over-dispersion to highlight relevant features.

For hypothesis testing, C-SIDE¹³ uses the Wald test, explicitly estimating $\boldsymbol{\beta}$ and computing significance via the Fisher Information at $\hat{\boldsymbol{\beta}}$.

Remark (score, LR and Wald tests): The score test is popular for variance-component testing because it is computationally efficient; It requires fitting only the null model once, even when evaluating high-dimensional covariates (e.g., genotypes¹⁴). In contrast, LR and Wald tests necessitate estimating coefficients $\hat{\boldsymbol{\beta}}$ under the alternative. While $\hat{\boldsymbol{\beta}}$ is necessary to interpret effect magnitude or direction (e.g., how spatial location may affect a gene’s expression), it is computationally superfluous for the task of *detection* (whether a gene is spatially variable or not). Given that score, LR, and Wald tests are asymptotically equivalent for local alternatives, the score test captures the same statistical signal without the overhead of fitting the generative model with covariates. General test agreement outside of $\boldsymbol{\beta} \approx \mathbf{0}$, as well as the quality of $\hat{\boldsymbol{\beta}}$, depends on the log-likelihood surface (which is usually well-behaved for common parametric families).

2.5.2 Generalized linear mixed models (GLMMs)

Finally, consider the GLMMs used in SPARK¹⁵ (Poisson) or GPcount¹⁶ (Negative Binomial),

$$g(\mathbb{E}[\mathbf{x}]) = b\mathbf{1} + \boldsymbol{\epsilon}, \quad \boldsymbol{\epsilon} \sim \mathcal{N}(\mathbf{0}, \boldsymbol{\Sigma}_\theta),$$

where the covariance is defined as $\boldsymbol{\Sigma}_\theta = \tau^2(\mathbf{I} + \theta\mathbf{K})$. Likelihood-based tests for $H_0 : \theta = 0$ rely on the marginal likelihood, which requires integrating out the random effects $\boldsymbol{\epsilon}$. Using Laplace approximation, the marginal becomes $l(\theta) = \ln \int f_g(\mathbf{x}|\boldsymbol{\epsilon})f_\theta(\boldsymbol{\epsilon})d\boldsymbol{\epsilon} \approx \ln f_g(\mathbf{x}|\hat{\boldsymbol{\epsilon}}_\theta) + \ln f_\theta(\hat{\boldsymbol{\epsilon}}_\theta)$ where $\hat{\boldsymbol{\epsilon}}_\theta =$

$\text{argmax}_{\epsilon} [f_g(\mathbf{x}|\epsilon) f_{\theta}(\epsilon)]$ is the posterior mode for a fixed θ . The total gradient of $l(\theta)$ now simplifies because the term involving the partial derivative with respect to the maximizer $\hat{\epsilon}_{\theta}$ vanishes,

$$\nabla_{\theta} l(\theta) \approx \frac{\partial l}{\partial \theta} + \underbrace{\frac{\partial l}{\partial \epsilon(\theta)} \frac{\partial \hat{\epsilon}(\theta)}{\partial \theta}}_{=0} = \frac{\partial}{\partial \theta} \ln f_{\theta}(\hat{\epsilon}_{\theta}).$$

Substituting the Gaussian log-density $\ln f_{\theta}(\epsilon) \propto -\frac{1}{2} \ln |\Sigma_{\theta}| - \frac{1}{2} \epsilon^{\top} \Sigma_{\theta}^{-1} \epsilon$ and noting that $\frac{\partial \Sigma_{\theta}}{\partial \theta}|_{\theta=0} = \tau^2 \mathbf{K}$, the gradient at the null becomes

$$\nabla_{\theta} l(\theta)|_{\theta=0} = -\frac{1}{2} \text{tr}(\Sigma_0^{-1}(\tau^2 \mathbf{K})) + \frac{1}{2} \hat{\epsilon}_0^{\top} \Sigma_0^{-1}(\tau^2 \mathbf{K}) \Sigma_0^{-1} \hat{\epsilon}_0 = \frac{1}{2} \left(\frac{1}{\tau^2} \hat{\epsilon}_0^{\top} \mathbf{K} \hat{\epsilon}_0 - \text{tr}(\mathbf{K}) \right)$$

since $\Sigma_0 = \tau^2 \mathbf{I}$. Similar to LMM's Eq. (6), here the score test also corresponds to a Q-statistic

$$Q_{\text{GLMM}} = \tilde{\mathbf{z}}^{\top} \mathbf{K} \tilde{\mathbf{z}}, \quad (8)$$

where $\tilde{\mathbf{z}} = \hat{\epsilon}_0 / \tau$ is the standardized posterior mode of the random effects under the null, which has zero mean and unit variance. Unlike Eq. (6) and Eq. (7), however, here $\tilde{\mathbf{z}}$ needs to be computed by maximizing the posterior. To further simplify the form, we note a direct connection between $\tilde{\mathbf{z}}$ and the standard GLM working residuals $\tilde{\mathbf{z}}_0 = \text{argmax}_{\epsilon} [\ln f_g(\mathbf{x} | b + \epsilon)]$. The GLMM mode $\tilde{\mathbf{z}}$ maximizes the penalized log-likelihood $\mathcal{Q}(\epsilon) = \ln f_g(\mathbf{x} | b + \epsilon) - \frac{1}{2\tau^2} |\epsilon|^2$. A second-order Taylor expansion of the likelihood term around $\tilde{\mathbf{z}}_0$ gives

$$\ln f_g(\mathbf{x} | b + \epsilon) \approx \text{const} - \frac{1}{2} (\epsilon - \tilde{\mathbf{z}}_0)^{\top} \mathcal{J}(\epsilon - \tilde{\mathbf{z}}_0),$$

where $\mathcal{J} = -\nabla_{\epsilon}^2 \ln f_g(\mathbf{x} | b + \tilde{\mathbf{z}}_0)$ is the observed information matrix of the GLM. Under the null hypothesis of i.i.d. \mathbf{x} entries, \mathcal{J} is diagonal with entries $\mathcal{J}_{ii} = \frac{1}{\text{Var}(x)[g'(\mu)]^2}$. Maximizing the approximate quadratic form thus yields the relationship

$$\tilde{\mathbf{z}} = \text{argmax}_{\epsilon} \mathcal{Q}(\epsilon) \approx \left(\frac{1}{\tau^2} \mathbf{I} + \mathcal{J} \right)^{-1} \mathcal{J} \tilde{\mathbf{z}}_0 = \frac{nv_0}{nv_0 + \tau^{-2}} \frac{\mathbf{x} - \mu_0}{v_0} = \frac{\mathbf{x} - \mu_0}{v_1}, \quad (9)$$

where $v_1 = v_0 + \frac{1}{n\tau^2}$ represents another variance estimator adjusted for the random effect prior.

Remark: The data transformation (from \mathbf{x} to \mathbf{z}) in Eq. (7) and Eq. (9) is *global* because the observations \mathbf{x} are i.i.d. under the null hypothesis. Computationally, the scalings v_0 and v_1 can be calculated directly from nuisance parameters (the sample mean $\bar{\mathbf{x}}$, dispersion r etc.). In a more general setting with covariates, \mathcal{J} is not a scaled identity matrix, making the transformation spot-specific. This distinction is important for cell-type-specific spatial variability testing in Section 2.8.

2.6 HSIC-based tests as Q-tests

Q-statistic can be rigorously understood as a special case of the Hilbert-Schmidt Independence Criterion (HSIC)^{17,18}. Using the convergence result of HSIC and general RKHS theory, we prove that all Q-tests can only detect mean-shift spatial variability (Theorem 1).

2.6.1 HSIC background

To motivate the kernel-based perspective, consider the simple case where we wish to test if a gene X is linearly dependent on spatial coordinates $S \in \mathbb{R}^d$. A natural statistic is the sum of squared covariances between X and each spatial coordinate. For standardized data \mathbf{z} , this is given by $|\mathbf{S}^{\top} \mathbf{z}|^2 = \mathbf{z}^{\top} \mathbf{S} \mathbf{S}^{\top} \mathbf{z}$, which is a Q-statistic where the kernel $\mathbf{K} = \mathbf{S} \mathbf{S}^{\top}$ is the linear kernel on spatial locations.

Gretton *et al.* [17] generalizes the notion of covariance to non-linear dependencies by mapping variables into RKHSs. Let \mathcal{F} and \mathcal{G} be RKHSs on \mathcal{X} and \mathcal{S} with kernels $l(\cdot, \cdot)$ and $k(\cdot, \cdot)$, respectively. The population HSIC is defined as the squared Hilbert-Schmidt norm of the cross-covariance operator Σ_{XS} ,

$$\text{HSIC}(P_{XS}, \mathcal{F}, \mathcal{G}) := |\Sigma_{XS}|_{\text{HS}}^2 = \|\mathbb{E}_{XS}[l(X, \cdot) \otimes k(S, \cdot)] - \mathbb{E}_X[l(X, \cdot)] \otimes \mathbb{E}_S[k(S, \cdot)]\|_{\mathcal{F} \otimes \mathcal{G}}^2.$$

Intuitively, HSIC measures the distance between the kernel mean embedding of the joint distribution and the product of its marginals. If the kernels are characteristic (universal), HSIC = 0 if and only if X and S are independent (i.e., no spatial variability).

2.6.2 Q-test is a kernel dependence test with a linear data kernel

In the context of spatial transcriptomics, **SPARK-X**¹⁹ and **SPLISOSM**¹ utilize the empirical estimator of HSIC. To maintain computational efficiency and interpretability, these methods typically employ a *linear* kernel for the gene expression domain ($l(x, x') = \langle x, x' \rangle$), while retaining a general spatial kernel $k(s, s')$ to capture complex spatial patterns. We have previously shown that any low-rank spatial kernel, including **SPARK-X**, leads to substantial power loss¹. Below, we expand our analysis to discuss the implications of using a linear data kernel on test consistency.

The HSIC-based test statistic for SVG is defined as

$$S_{\text{HSIC}} = \frac{1}{(n-1)^2} \text{tr}(\mathbf{KHLH}),$$

where \mathbf{K} is the spatial kernel matrix $K_{ij} = k(s_i, s_j)$, $\mathbf{L} = \mathbf{xx}^\top$ is the linear kernel matrix for expression, and $\mathbf{H} = \mathbf{I} - \frac{1}{n}\mathbf{1}\mathbf{1}^\top$ is the centering matrix. Substituting \mathbf{L} into the equation reveals the equivalence to the Q-statistic as

$$S_{\text{HSIC}} \propto \text{tr}(\mathbf{KHxx}^\top \mathbf{H}) = \mathbf{x}^\top \mathbf{HKHx} \propto \mathbf{z}^\top \mathbf{Kz} = Q_{\text{HSIC}}. \quad (10)$$

This derivation provides a second interpretation of the Q-statistic, complementary to the LMM perspective (Section 2.4.2, where Q_n measures the fit to a spatial prior). The HSIC perspective interprets Q as a measure of *generalized covariance*. By Mercer's Theorem, the positive semi-definite kernel \mathbf{K} can be decomposed as $\mathbf{K} = \Phi\Phi^\top$, where $\Phi \in \mathbb{R}^{n \times m}$ represents the spatial coordinates transformed into a high-dimensional feature space (where m may be infinite). The Q-statistic essentially measures the norm of $\Phi^\top \mathbf{z}$, an extension of the standard Pearson correlation.

2.6.3 Linear data kernel restricts Q-test consistency to mean dependence

The kernel perspective also allows us to apply RKHS theory to analyze test properties. Gretton *et al.* [18] showed that the empirical HSIC in Eq. (10) is a consistent estimator of the population HSIC. Consequently, a standard HSIC test using two universal kernels (which the linear kernel is not) is consistent against *all* forms of dependence. However, the use of linear expression kernel limits the sensitivity of the test, leading to the following consistency result:

Theorem 1 (Q-statistic measures mean dependence). *Let \mathcal{H}_S be a RKHS on the spatial domain \mathcal{S} associated with a characteristic kernel $k(\cdot, \cdot)$. Let \mathcal{H}_X be the RKHS on the expression domain $\mathcal{X} \subseteq \mathbb{R}$ associated with the linear kernel $l(x, x') = \langle x, x' \rangle$. We define the population Q-statistic, Q , as the HSIC between S and X under these kernels*

$$Q(P_{SX}) := \text{HSIC}(P_{SX}, \mathcal{H}_S, \mathcal{H}_X) = |C_{SX}|_{HS}^2. \quad (11)$$

Then, $Q(P_{SX}) = 0$ if and only if X is mean independent of S ; that is,

$$\mathbb{E}[X | S] = \mathbb{E}[X] \quad \text{almost surely.} \quad (12)$$

Proof. The squared Hilbert-Schmidt norm of the cross-covariance operator C_{SX} vanishes if and only if the operator is null. That is, for all $f \in \mathcal{H}_S$ and $g \in \mathcal{H}_X$, the covariance is

$$\langle f, C_{SX}g \rangle_{\mathcal{H}_S} = \text{Cov}[f(S), g(X)] = \mathbb{E}[f(S)g(X)] - \mathbb{E}[f(S)]\mathbb{E}[g(X)] = 0.$$

Since \mathcal{H}_X is generated by a linear kernel, any function $g \in \mathcal{H}_X$ is a linear functional of the form $g(x) = \langle v, x \rangle$ for some vector $v \in \mathbb{R}^d$. Substituting this into the covariance condition yields

$$\mathbb{E}[f(S)\langle v, X \rangle] = \mathbb{E}[f(S)]\mathbb{E}[\langle v, X \rangle] \quad \forall f \in \mathcal{H}_S, \forall v \in \mathbb{R}^d. \quad (13)$$

By the law of total expectation, we can rewrite the left side as

$$\text{LHS} = \mathbb{E}_S[f(S)\mathbb{E}_X[\langle v, X \rangle | S]] = \mathbb{E}[f(S)]\langle v, \mathbb{E}[X | S] \rangle.$$

Substituting it back to Eq. (13) and using the linearity of the inner product, the condition becomes

$$\mathbb{E}_S[f(S)(\langle v, \mathbb{E}[X | S] \rangle - \langle v, \mathbb{E}[X] \rangle)] = 0 \quad \forall f \in \mathcal{H}_S, \forall v \in \mathbb{R}^d.$$

Since k is a characteristic kernel, the embedding $\mu: P \rightarrow \int k(\cdot, s)dP(s)$ is injective. This implies that if $\mathbb{E}[f(S)h(S)] = 0$ for all $f \in \mathcal{H}_S$, then $h(S) = 0$ almost surely. Therefore, we must have

$$\langle v, \mathbb{E}[X | S] - \mathbb{E}[X] \rangle = 0 \quad \text{a.s.}$$

Since this must hold for any arbitrary vector v , it follows that $\mathbb{E}[X | S] = \mathbb{E}[X]$ almost surely. \square

Mean independence is a strictly weaker condition than the statistical independence ($P(X | S) = P(X)$) required by Definition 2.1. Consequently, Theorem 1 implies that Q-tests are insensitive to “higher-order” spatial variability, such as pure spatial heteroscedasticity where the mean is constant but the variance changes (e.g., $\mathbb{E}[X | S] = \mu$ but $\text{Var}(X | S) = g(S)$).

Remark: This limitation must not be confused with the structure of random effects models where spatial dependence is modeled via a covariance matrix (Eq. (5)). While the spatial random effect has a prior expectation of zero, its realization $\phi(s)$ acts as a spatially varying intercept, effectively shifting $\mathbb{E}[X | S = s]$. The residual noise variance σ (from the white noise) remains homoscedastic.

Corollary 1.1 (Q-test consistency). *The Q-test is consistent against the specific class of alternatives defined by spatial mean dependence. That is, if the alternative hypothesis is*

$$H_1: \mathbb{E}[X | S] \neq \mathbb{E}[X] \quad \text{on a set of non-zero measure,}$$

then the power of the test approaches 1 as $n \rightarrow \infty$.

Proof. Under the alternative H_1 , Theorem 1 establishes that the population statistic $Q(P_{SX}) > 0$. The Q-test consistency is thus a special case of the general HSIC test consistency shown in Gretton *et al.* [18], using the fact that the empirical HSIC estimator converges in probability to the population HSIC (in our case, $|\frac{1}{n^2}Q_n - Q(P_{SX})| \xrightarrow{d} 0$) as $n \rightarrow \infty$ under H_1 , and that $\frac{1}{n}Q_n$ converges to a constant distribution (weighted χ^2 mixture, a property of the V-statistic) under H_0 . \square

We note that the blindness of the Q-test to higher-order dependence can be rectified by replacing the linear expression kernel with a characteristic one (e.g., Gaussian), albeit at a higher computational cost. However, as will be discussed in Supplementary Note 3, this is often unnecessary for spatial omics data. Furthermore, the linear kernel is not the only transformation that compresses information about X ; for instance, a popular expression binarization procedure, adopted by many SVG detection tools like BinSpect²⁰, similarly reduces the full distribution $P(X)$ to its mean $P(X = 1)$.

2.7 Other dependence-based spatial variability tests

In this section, we review the remaining SVG detection methods categorized as “dependence-based” by Yan *et al.* [21] that were not previously discussed (e.g., those not based on Moran’s I or non-HSIC variants). **This is not an exhaustive list of all published SVG detection tools.** Rather, we hope that some of the underlying principles analyzed here can be generalized to a broader class of methods, even beyond the scope of spatial pattern detection.

2.7.1 Relationship between Mutual Information (MI) and HSIC

HSIC is not the only metric that directly evaluates Definition 2.1. One common alternative is Mutual Information (MI), formally the Kullback-Leibler (KL) divergence between the joint density and the product of marginals. Estimating MI requires evaluating the log-ratio of densities, a task that is

notoriously difficult in high dimensions. HSIC offers a computationally tractable alternative that can be interpreted through the lens of Kernel Density Estimators (KDEs).

Let \mathcal{H}_S and \mathcal{H}_X be RKHSs with kernels k and l , respectively. We construct KDEs for the marginals and the joint distribution using these kernels as

$$\hat{f}_X(x) = \frac{1}{n} \sum_{i=1}^n l(x, x_i), \quad \hat{f}_S(s) = \frac{1}{n} \sum_{i=1}^n k(s, s_i), \quad \hat{f}_{XS}(x, s) = \frac{1}{n} \sum_{i=1}^n l(x, x_i)k(s, s_i).$$

The empirical HSIC statistic is exactly the squared norm of the difference between the joint KDE and the product of the marginal KDEs within the product RKHS $\mathcal{H}_X \otimes \mathcal{H}_S$

$$\text{HSIC}_n = \left\| \hat{f}_{XS} - \hat{f}_X \hat{f}_S \right\|_{\mathcal{H}_X \otimes \mathcal{H}_S}^2. \quad (14)$$

To see the connection between MI and Eq. (14), consider the density ratio $r(x, s) := \frac{\hat{f}_{XS}}{\hat{f}_X \hat{f}_S}(x, s)$. Using the Taylor expansion of $\log(r(x, s))$ at $r \approx 1$ (representing almost independence), the KL divergence can be approximated by the Pearson χ^2 -divergence, yielding

$$I(X; S) \approx \frac{1}{2} \int \int \frac{(\hat{f}_{XS} - \hat{f}_X \hat{f}_S)^2(x, s)}{\hat{f}_X(x) \hat{f}_S(s)} dx ds. \quad (15)$$

Eq. (14) and Eq. (15) differ in weighting. HSIC measures the squared difference directly, treating high-density and low-density regions with equal weight, whereas KL penalizes deviations in low-probability regions more heavily (due to the log).

Remark: In the specific case of the Q-statistic, where \mathcal{H}_X uses the linear kernel $l(x, x') = \langle x, x' \rangle$, \hat{f}_X is not a valid probability density but rather the mean embedding. Consequently, the distance $|\hat{f}_{XS} - \hat{f}_X \hat{f}_S|^2$ collapses from a comparison of densities to a comparison of conditional expectations. This is another explanation on why using the linear kernel reduces the test from detecting general dependence (like KL) to detecting only mean dependence (Theorem 1).

2.7.2 BinSpect (Dries et al., 2021)

BinSpect²⁰ from the Giotto toolbox uses a binarized representation of gene expression: $\mathbf{x} \in \{0, 1\}^n$. Given a spatial network (here represented by its adjacency matrix \mathbf{W}), BinSpect tallies up the edges that join up pairs of 0-0, 0-1, 1-0, and 1-1 vertices, constructs the (2×2) -contingency table, and reports the associated odds ratio and p -value from Fisher's exact test. The entries of this contingency table can be expressed in vector notation as

$$\begin{aligned} n_{11} &= \mathbf{x}^\top \mathbf{W} \mathbf{x}, & n_{10} &= \mathbf{x}^\top \mathbf{W} (\mathbf{1} - \mathbf{x}), \\ n_{01} &= (\mathbf{1} - \mathbf{x})^\top \mathbf{W} \mathbf{x}, & n_{00} &= (\mathbf{1} - \mathbf{x})^\top \mathbf{W} (\mathbf{1} - \mathbf{x}). \end{aligned}$$

The odds ratio $\frac{n_{00}n_{11}}{n_{01}n_{10}}$ is closely related to the χ^2 -statistic, which serves as a common approximation to Fisher's exact test. Conditional on the margin totals, the χ^2 -statistic is

$$\chi^2 = \frac{n(n_{00}n_{11} - n_{01}n_{10})^2}{(n_{00} + n_{01})(n_{10} + n_{11})(n_{00} + n_{10})(n_{10} + n_{11})},$$

so that the odds ratio is 1 iff $\chi^2 = 0$. Furthermore, by substituting in the expression for the entries of the contingency table, $\Delta := n_{00}n_{11} - n_{01}n_{10}$ can be rewritten as a quadratic form involving the graph structure. Let $m = \mathbf{1}^\top \mathbf{W} \mathbf{1}$ be the total weight (or number of edges) and $\mathbf{k} = \mathbf{W} \mathbf{1}$ be the degree vector. We have

$$\begin{aligned} \Delta &= (\mathbf{x}^\top \mathbf{W} \mathbf{x})((\mathbf{1} - \mathbf{x})^\top \mathbf{W} (\mathbf{1} - \mathbf{x})) - (\mathbf{x}^\top \mathbf{W} (\mathbf{1} - \mathbf{x}))((\mathbf{1} - \mathbf{x})^\top \mathbf{W} \mathbf{x}) \\ &= (\mathbf{x}^\top \mathbf{W} \mathbf{x})(\mathbf{1}^\top \mathbf{W} \mathbf{1}) - (\mathbf{x}^\top \mathbf{W} \mathbf{1})(\mathbf{1}^\top \mathbf{W} \mathbf{x}) \\ &= m(\mathbf{x}^\top \mathbf{W} \mathbf{x}) - (\mathbf{x}^\top \mathbf{k})(\mathbf{k}^\top \mathbf{x}) \\ &= \mathbf{x}^\top (m\mathbf{W} - \mathbf{k}\mathbf{k}^\top) \mathbf{x}. \end{aligned}$$

The matrix $\mathbf{M} = m\mathbf{W} - \mathbf{k}\mathbf{k}^\top$ is a scaled version of the *modularity matrix* $\mathbf{B} = \mathbf{W} - \frac{1}{m}\mathbf{k}\mathbf{k}^\top$ used in community detection. Thus, the **BinSpect** statistic is equivalent to calculating the modularity of the spatial graph given the partition induced by the binarized gene expression

$$Q_{\text{BinSpect}} = \mathbf{x}^\top \mathbf{M} \mathbf{x} \equiv (\mathbf{x} - \bar{\mathbf{x}})^\top \mathbf{M} (\mathbf{x} - \bar{\mathbf{x}}).$$

Note that the data \mathbf{x} is binarized separately for each gene using the same criterion (e.g., k -means with 2 clusters, or rank thresholding at 30%). The mean $\bar{\mathbf{x}}$ and the missing variance scalar in Q_{BinSpect} are thus almost constant across genes and do not affect gene ranking.

Remark: The spectrum of the modularity matrix has been well-studied. In particular: (i) $\mathbf{1}$ is in the null space (eigenvalue 0), (ii) eigenvalues are interlaced with those of \mathbf{W} , (iii) the sum of eigenvalues is negative, and (iv) the number of positive eigenvalues is related to the number of communities. Consequently, we expect that cancellation will occur (to a similar degree as methods that use the weight matrix \mathbf{W} directly, like Moran's I).

Remark: The denominator in the χ^2 is a kind of normalization by the variance of \mathbf{x} . To wit, assuming that \mathbf{W} is symmetric, the denominator is

$$\frac{(\mathbf{k}^\top \mathbf{x})^2 (\mathbf{k}^\top (\mathbf{1} - \mathbf{x}))^2}{n} = \frac{(m\mu)^2 (m(1 - \mu))^2}{n} = \frac{m^4}{n} (\mu(1 - \mu))^2,$$

where $\mu = \frac{\mathbf{k}^\top \mathbf{x}}{m}$ is the degree-weighted mean of \mathbf{x} . Furthermore, for a binary vector, the degree-weighted variance is $\mu(1 - \mu)$.

2.7.3 trendsceek (Edsgard et al., 2018)

trendsceek²² uses various two-point statistics for marked point processes to detect spatial expression trends. These statistics compare the dependency between expression values ($\mathbf{x} = [x_1, \dots, x_n]^\top$) at two locations (s_i, s_j) conditioned on the distance $d(s_i, s_j) = r$. Specifically, they propose:

(a) Stoyan's mark-correlation:

$$\rho(r) = \frac{\mathbb{E}[x_i x_j \mid d(s_i, s_j) = r]}{\mathbb{E}[x_i x_j]}$$

(b) Mark-variogram:

$$\gamma(r) = \frac{\mathbb{E}[(x_i - x_j)^2 \mid d(s_i, s_j) = r]}{2}.$$

(c) Mean-mark:

$$E(r) = \mathbb{E}[x_i \mid d(s_i, s_j) = r]$$

(d) Variance-mark:

$$V(r) = \mathbb{E}[(x_i - E(r))^2 \mid d(s_i, s_j) = r] = \mathbb{E}[x_i^2 \mid d(s_i, s_j) = r] - E(r)^2$$

For each of these statistics $Q \in \{\rho, E, V, \gamma\}$, they compare the observed value of these statistics to the expected value under the null distribution obtained by permuting expression values

$$\Delta_Q(r) = |Q(r) - Q^{\text{exp}}(r)|.$$

Estimation of these spatial statistics from data requires density estimation, as implemented in **spatstat**²³. To cast them into our quadratic form framework, we define a distance-based spatial weight matrix $\mathbf{W}^{(r)}$. In the simplest case (box kernel), $\mathbf{W}_{ij}^{(r)} = \frac{1}{|\mathcal{P}_r|}$ if $d(s_i, s_j) \approx r$ and 0 otherwise, where $|\mathcal{P}_r|$ is the number of pairs at distance r . More generally, $\mathbf{W}^{(r)}$ represents a kernel smoother centered at r . For simplicity, let us fix $r > 0$, assume there are ample pairs in the set \mathcal{P}_r , and that $\mathbf{W}^{(r)}$ is symmetric. The statistics are estimated as follows:

(a) The estimate of mark-correlation is:

$$\hat{\rho}(r) = \frac{\sum_{i,j} \mathbf{W}_{ij}^{(r)} x_i x_j}{\frac{1}{n^2} \sum_{i,j} x_i x_j} = \frac{\mathbf{x}^\top \mathbf{W}^{(r)} \mathbf{x}}{\mathbf{x}^\top \mathbf{B} \mathbf{x}}.$$

This is a Rayleigh quotient with $\mathbf{B} = \frac{1}{n^2} \mathbf{1} \mathbf{1}^\top$. The deviation from the expected mean is thus

$$\Delta_\rho(r) = \left| \frac{\mathbf{x}^\top \mathbf{W}^{(r)} \mathbf{x}}{\mathbf{x}^\top \mathbf{B} \mathbf{x}} - 1 \right| \propto \left| \mathbf{x}^\top (\mathbf{W}^{(r)} - \mathbf{B}) \mathbf{x} \right|.$$

In Edsgård *et al.* [22], a ranking procedure is proposed in which the expression values are permuted several times and the statistic is recomputed for each permuted dataset, from which a p -value is computed from ranking the statistic on actual data against the statistics on permuted data. Note that the denominator in the Rayleigh quotient above is permutation-invariant, and hence does not affect the rankings produced by the method.

(b) With $\mathbf{W} = \mathbf{W}^{(r)}$, the estimated mark-variogram is

$$\hat{\gamma}(r) = \frac{1}{2} \sum_{i,j} \mathbf{W}_{ij} (x_i - x_j)^2 = \mathbf{x}^\top \mathbf{L}_\mathbf{W} \mathbf{x},$$

where $\mathbf{L}_\mathbf{W} = \mathbf{D}_\mathbf{W} - \mathbf{W}$ is the Laplacian matrix associated with \mathbf{W} . The expected statistic is $\mathbf{x}^\top \mathbf{L}_\mathbf{B} \mathbf{x}$, where $\mathbf{L}_\mathbf{B}$ is the Laplacian associated with \mathbf{B} . Hence the deviation is

$$\Delta_\gamma(r) = \left| \mathbf{x}^\top (\mathbf{L}_\mathbf{W} - \mathbf{L}_\mathbf{B}) \mathbf{x} \right|.$$

(c) With $\mathbf{W} = \mathbf{W}^{(r)}$, the estimated mean-mark is

$$\hat{E}(r) = \sum_{i,j} \mathbf{W}_{ij} x_i = \mathbf{1}^\top \mathbf{W} \mathbf{x}.$$

Hence the expected deviation is $\Delta_E(r) = \left| \mathbf{1}^\top (\mathbf{W} - \mathbf{B}) \mathbf{x} \right|$. While this is not a quadratic form, its square is

$$\Delta_E(r)^2 = \mathbf{x}^\top \boldsymbol{\delta} \boldsymbol{\delta}^\top \mathbf{x},$$

where $\boldsymbol{\delta} = \mathbf{W}^\top \mathbf{1} - \mathbf{B}^\top \mathbf{1}$ is the difference of the degree vectors.

(d) The estimated variance-mark is

$$\hat{V}(r) = \sum_{i,j} \mathbf{W}_{ij} x_i^2 - \left(\sum_{i,j} \mathbf{W}_{ij} x_i \right)^2 = \mathbf{x}^\top (\mathbf{D}_\mathbf{W} - \mathbf{k} \mathbf{k}^\top) \mathbf{x},$$

where $\mathbf{k} = \mathbf{W}^\top \mathbf{1}$ is the column degree vector. Denoting the kernel $\mathbf{K}_\mathbf{W} = \mathbf{D}_\mathbf{W} - \mathbf{k} \mathbf{k}^\top$ and similarly $\mathbf{K}_\mathbf{B}$ for \mathbf{B} , we have

$$\Delta_V(r) = \left| \mathbf{x}^\top (\mathbf{K}_\mathbf{W} - \mathbf{K}_\mathbf{B}) \mathbf{x} \right|.$$

In summary, all four metrics in `trendsceek` reduce to comparing a specific quadratic form $\mathbf{x}^\top \mathbf{K}^{(r)} \mathbf{x}$ against a null quadratic form derived from the global distribution. The kernels $\mathbf{K}^{(r)}$ for mark-variogram, mean-mark and variance-mark (but not mark-correlation) are double-centered, meaning that the test statistics do not depend on the mean of \mathbf{x} , thus connecting to the standardized data \mathbf{z} .

Indeed, from a kernel design perspective these four statistics (for fixed r) uses well-known constructions: weight matrices, Laplacian matrices, and mean-field approximations thereof. What is particularly interesting about these spatial statistics is that the weight matrices generalize the usual weight matrix $\mathbf{W}^{(0)}$ which is peaked for nearby points ($r = 0$) and instead consider a family of such matrices that are sensitive to points at a specific distance $r \in [0, \infty)$. However, once $r > 0$, we see that $\mathbf{W}^{(r)}$ has trace zero, and as a consequence has both positive and negative eigenvalues (if not identically zero). The Laplacian $\mathbf{L}^{(r)}$ fares better: its eigenvalues are all non-negative and it avoids the risk of cancellation.

2.7.4 singleCellHaystack (Vandenbon et al., 2020)

singleCellHaystack²⁴ uses an information-theoretic measure to quantify the independence of cell spatial and expression distributions. More precisely, they consider a distribution Q of all cells in the space, along with distributions P_0, P_1 of cells in space with undetectable or detected expression of a gene ($x_i \in \{0, 1\}$), and define the divergence of the gene to be:

$$D_{KL} = \text{KL}(P_0 \| Q) + \text{KL}(P_1 \| Q),$$

where KL is the Kullback-Leibler divergence. The distributions Q, P_0, P_1 are estimated from finite samples $\{(x_i, s_i)\}$ as mixtures and can be parametrized by their mixture weights $\mathbf{y} \in [0, 1]^n$ (normalized to have sum one): given a spatial grid with grid points p , the density is $f_{\mathbf{y}}(p) = \sum_i y_i h(s_i, p) =: \mathbf{y}^\top \mathbf{h}(p)$. With this notation, the density estimate of Q is given by $f_{\frac{1}{n}}$; the density estimate of P_0 (resp. P_1) is given by $f_{\frac{1-\mathbf{x}}{n-\|\mathbf{x}\|_1}}$ (resp. $f_{\frac{\mathbf{x}}{\|\mathbf{x}\|_1}}$). (In the original method, $h(s, p) \propto e^{-d(s, p)^2/2}$, but the precise form doesn't matter for our result.)

From the discussion in Section 2.7.1, we can approximate the KL divergence, and hence D_{KL} , by quadratic forms. More specifically, if \mathbf{y} and \mathbf{y}' are two sets of mixture weights, then

$$\text{KL}(f_{\mathbf{y}'} \| f_{\mathbf{y}}) \approx (\mathbf{y}' - \mathbf{y})^\top \mathbf{K}(\mathbf{y}' - \mathbf{y}) + O(\|\mathbf{y}' - \mathbf{y}\|_2^3),$$

where $\mathbf{K}_{ij} = \frac{1}{2} \sum_p \frac{h(s_i, p)h(s_j, p)}{\mathbf{y}^\top \mathbf{h}(p)}$ is related to the Fisher information metric.

Substituting in the mixture weights, we have

$$\begin{aligned} \text{KL}(P_0 \| Q) &\approx \mathbf{z}^{(0)\top} \mathbf{K} \mathbf{z}^{(0)}, \\ \text{KL}(P_1 \| Q) &\approx \mathbf{z}^{(1)\top} \mathbf{K} \mathbf{z}^{(1)}, \\ D_{KL} &\approx \mathbf{z}^{(0)\top} \mathbf{K} \mathbf{z}^{(0)} + \mathbf{z}^{(1)\top} \mathbf{K} \mathbf{z}^{(1)}, \end{aligned}$$

where

$$\begin{aligned} \mathbf{z}^{(0)} &= \frac{\mathbf{1} - \mathbf{x}}{n - \|\mathbf{x}\|_1} - \frac{\mathbf{1}}{n}, \\ \mathbf{z}^{(1)} &= \frac{\mathbf{x}}{\|\mathbf{x}\|_1} - \frac{\mathbf{1}}{n}, \\ \mathbf{K}_{ij} &= \frac{1}{2} \cdot \sum_p \frac{h(s_i, p)h(s_j, p)}{\sum_k h(s_k, p)}. \end{aligned}$$

Furthermore, observe that $\mathbf{z}^{(0)} = -\frac{\|\mathbf{x}\|_1}{n - \|\mathbf{x}\|_1} \mathbf{z}^{(1)}$, so that we may simplify:

$$D_{KL} \approx \left(1 + \left(\frac{\|\mathbf{x}\|_1}{n - \|\mathbf{x}\|_1} \right)^2 \right) \mathbf{z}^{(1)\top} \mathbf{K} \mathbf{z}^{(1)}$$

Up to scaling, \mathbf{K} is a Nyström-like low-rank approximation based on landmarks of (a weighted version of) the kernel h , and therefore shares some of the same spectral properties of $h(s_i, s_j)$. For example, if h is the Gaussian kernel as in the original method, then \mathbf{K} approximates the Gaussian/RBF kernel. The matrix \mathbf{K} is positive semidefinite, and has no zero eigenvalues provided the rectangular matrix with entries $h(s_i, p)$ has full rank, which is true for most choices of density kernel h and when the grid is sufficiently large ($\geq n$ points). However, by default singleCellHaystack uses only 100 landmark points as the grid, which is typically fewer than the number of cells, and hence introduces “blind spots”, though hopefully innocuous by choice of grid construction.

2.8 Q-tests for cell-type-specific spatial variability testing

In many biological contexts, spatial patterns may be driven by confounding factors, such as cell-type distribution. For instance, a gene may appear spatially variable simply because it is a marker for a cell type that is spatially clustered. To distinguish intrinsic spatial regulation from confounding effects, we introduce conditional spatial variability.

Definition 2.3 (Conditional Spatial Variability). Let C be a confounding random variable (e.g., cell-type). We say X exhibits conditional spatial variability given C if X and S are conditionally dependent given C . Formally, the null hypothesis of conditional independence ($X \perp\!\!\!\perp S | C$) implies,

$$f_{X|S,C}(x|s, c) = f_{X|C}(x|c), \quad \forall x, s, c.$$

Conversely, X is conditionally spatially variable if this equality fails for a set of c with non-zero probability.

For completeness, we discuss tests designed to detect spatial variability within a given cell type. Note as resolution of spatial transcriptomics platforms keeps improving, at near single-cell level, the cell type indicator C is almost binary, and conditional spatial variability $X \perp\!\!\!\perp S | C$ can be simply determined by running the general spatial variability test on selected cells of the designed cell type ($c_i = 1$).

As far as we are aware, current existing approaches to identify cell-type-specific spatially variable genes are given explicitly as parametric models that incorporate spatial variability and cell-level variability (i.e., cell type proportions). A prototypical method of this form is C-SIDE¹³, which has already been discussed in section 2.5.1, but we spell out the model in greater detail here to appreciate how cell types are modeled. Suppose we have K cell types $k \in \{1, 2, \dots, K\}$. Then,

$$\begin{aligned} x_i | \lambda_i &\sim \text{Poisson}(n_i \lambda_i) \\ \log \lambda_i &= \log \left(\sum_{k=1}^K \pi_{ik} \mu_{ik} \right) + \epsilon_i \\ \log \mu_{ik} &= \alpha_{k0} + \sum_{l=1}^L \alpha_{kl} h_l(s_i) \end{aligned}$$

where $\{(x_i, s_i)\}$ is the spatially resolved transcriptomic data as before, n_i is a library size factor at spot s_i , λ_i is the size-normalized expression rate, π_{ik} is the proportion of cell type k at spot s_i , μ_{ik} is the cell-type-specific expression rate, and $\epsilon_i \sim N(0, \sigma^2)$ is a noise term. Furthermore, the cell-type-specific expression rate μ_{ik} is decomposed into a spatially invariant term α_{k0} , and contributions α_{kl} that depend on covariates $h_l(s_i)$ encoding transformations of spatial coordinates.

Ostensibly, this theoretical framework permits simultaneous inference of cell-type proportions and (cell-type-specific) spatial variability. However, practically these methods treat (spatial) cell-type deconvolution as a separate step (e.g., using RTCD²⁵) and infers the cell-type-specific weights α_{kl} using the estimated proportions $\hat{\pi}_{ik}$ as plugin estimators. In this case, the problem reduces entirely to the case of generalized linear models discussed above. One drawback of this two-step approach is that by considering cell-type proportions as fixed instead of inferred with uncertainty, the variance of the estimator of cell-type-specific weights may become biased.

We can dissect the resulting Q-test into a contribution from the cell-type proportions and a contribution from the spatial structure. The model is complex, so we resort to quasilikelihoods and quasiscores and approximate liberally. Under the null hypothesis $H_0 : \alpha_{kl} = 0$ for all $k \in \{1, \dots, K\}$ and $l \in \{1, \dots, L\}$, and conditioning on $\{n_i\}$, $\{\pi_{ik}\}$, $\{\alpha_{k0}\}$, and σ^2 , we have

$$\begin{aligned} m_i &:= \mathbb{E}[x_i | H_0] = n_i \sum_k \pi_{ik} e^{\alpha_{k0}} \\ v_i &:= \text{Var}(x_i | H_0) = m_i + m_i^2 (e^{\sigma^2} - 1) \end{aligned}$$

If instead α_{kl} are merely small, then linearizing near $\alpha \approx 0$ we find that

$$\mathbb{E}[x_i] \approx m_i + m_i \sum_{k,l} w_{ik} \alpha_{kl} h_l(s_i),$$

where $w_{ik} := \frac{\pi_{ik} e^{\alpha_{k0}}}{\sum_k \pi_{ik} e^{\alpha_{k0}}}$ is a kind of soft assignment of spot s_i to cell types.

Define the $(N \times KL)$ -matrix Φ by $\Phi_{i,k,l} = m_i w_{ik} h_l(s_i)$. We have $\mathbb{E}[\mathbf{x}] \approx \mathbf{m} + \Phi \alpha$. Setting $\mathbf{V} = \text{diag}(\mathbf{v})$, the quasiscore is $\mathbf{U} = \Phi^\top \mathbf{V}^{-1}(\mathbf{x} - \mathbf{m})$. With $\mathbf{z} = \mathbf{V}^{-1/2}(\mathbf{x} - \mathbf{m})$, the associated kernel score test statistic is

$$T = \mathbf{U}^\top \mathbf{U} = \mathbf{z}^\top \mathbf{V}^{-1/2} \Phi \Phi^\top \mathbf{V}^{-1/2} \mathbf{z},$$

where the kernel $\mathbf{K} = \mathbf{V}^{-1/2} \Phi \Phi^\top \mathbf{V}^{-1/2}$ is given by $\mathbf{K}_{ij} = \frac{m_i m_j}{\sqrt{v_i v_j}} \sum_{k,l} w_{ik} w_{jk} h_l(s_i) h_l(s_j)$. In particular, if we set $\mathbf{\Pi}_{ik} = m_i w_{ik}$ and $\mathbf{H}_{il} = h_l(s_i)$, then

$$\mathbf{K} = \mathbf{V}^{-1/2} (\mathbf{\Pi} \mathbf{\Pi}^\top \circ \mathbf{H} \mathbf{H}^\top) \mathbf{V}^{-1/2},$$

where \circ is the Hadamard product. The term $\mathbf{\Pi} \mathbf{\Pi}^\top$ is the contribution from cell type proportions, which is modifying the spatial kernel $\mathbf{H} \mathbf{H}^\top$.

For instance, if there is no variability in spot-level covariates (library sizes, cell-type proportions, etc.), then $\mathbf{\Pi} \mathbf{\Pi}^\top$ is a scalar multiple of $\mathbf{1} \mathbf{1}^\top$, so $\mathbf{\Pi} \mathbf{\Pi}^\top \circ \mathbf{H} \mathbf{H}^\top$ is a scalar multiple of $\mathbf{H} \mathbf{H}^\top$, and this cell-type-specific spatial variability reduces to an ordinary spatial variability. Similarly, if each spot consists of one (known) cell type ($\pi_{ik} = 1$ if spot s_i consists entirely of cell type k , and is 0 otherwise), then $\mathbf{\Pi} \mathbf{\Pi}^\top$ is a block diagonal matrix, with each block corresponding to a particular cell type, and the test statistic above decomposes as a (weighted) sum of the statistics that test in each cell type individually.

Other methods can be treated similarly. They differ from C-SIDE by assuming a different emission probability distribution (e.g., zero-inflated negative binomial instead of Poisson for CTSV²⁶), different functional forms relating λ_i to μ_{ik} , or different ways by which spatial information is encoded (e.g., spVC²⁷ uses learned splines). Observe that the parametric form of C-SIDE from above results in the spatial information “entering” as a linear kernel. Recent approaches such as STANCE²⁸, Celina²⁹, and MMM³⁰ use more general (e.g., distance-based) kernels \mathbf{K}' directly instead of linear kernels.

Spectrally, with notation as above, $\mathbf{\Pi} \mathbf{\Pi}^\top$ is positive-semidefinite; thus, if \mathbf{K}' is positive-semidefinite, then so is $\mathbf{\Pi} \mathbf{\Pi}^\top \circ \mathbf{K}'$ by Schur’s product theorem. If moreover \mathbf{K}' is positive-definite, then $\mathbf{\Pi} \mathbf{\Pi}^\top \circ \mathbf{K}'$ is also positive-definite by Oppenheim’s inequality and the fact that $(\mathbf{\Pi} \mathbf{\Pi}^\top)_{ii} > 0$ for all i . Therefore, despite the diversity, the underlying behavior of these cell-type-specific spatial variability methods in large part mirrors that of the non-cell-type-specific methods discussed before, by introducing a cell-type proportion induced weighting of the ordinary spatial structure kernels that preserves their spectral properties.

Supplementary Note 3 Functional and Spectral Analysis of Q-tests

Theorem 1 suggests that Q-tests—and SVG detection methods that reduce to them—are limited to detecting a single class of spatial variability: mean dependence. This limitation arises because the expression distribution $P(X|S)$ is effectively reduced to its mean. However, in applications such as spatial transcriptomics, this distributional information is *absent* because we observe only a single realization (x_i, s_i) drawn from $X | S = s_i$ at each location. This constraint blurs the line between mean independence and statistical independence. For example, given fixed samples from n unique locations, it is empirically impossible to distinguish between a random process $x_i \sim P(X)$ (no spatial variability) and a deterministic function $x_i = f(s_i)$ (spatial variability).

Motivated by this observation, this note adopts a functional perspective, treating the “signal” as a deterministic element of a Hilbert space. Using the spectrum theory of kernel operators, we derive conditions for test consistency regarding mean dependence (i.e., the functional alternative, Theorem 2) and discuss design principles to improve the power of spatial pattern detection.

3.1 A functional view of spatial patterns

We begin by formally defining spatial patterns as functions.

Definition 3.1 (Spatial Pattern). *Let \mathcal{S} be a compact spatial domain. A spatial pattern is a deterministic function $f \in L^2(\mathcal{S})$, the Hilbert space of square-integrable functions ($\int_{\mathcal{S}} |f(s)|^2 ds < \infty$) equipped with the inner product $\langle f, g \rangle = \int_{\mathcal{S}} f(s)g(s)ds$.*

The deterministic nature of this definition stands in contrast to the spatial random process perspective (Definition 2.1). For any finite realization of (X, S) , even if $X \perp\!\!\!\perp S$, there exists infinite many deterministic patterns f such that $x_i = f(s_i)$.

For spatial variability testing, the null hypothesis corresponds to $f(s) = c$ (constant almost everywhere). The alternative hypothesis encompasses all non-constant functions in $L^2(\mathcal{S})$, aligning with the mean dependence condition described in Corollary 1.1.

Definition 3.2 (Spatial Kernel Operators). *Let $k(\cdot, \cdot) \in L^2(\mathcal{S} \times \mathcal{S})$ be a symmetric function.*

1. *The spatial kernel operator $\mathcal{K} : L^2(\mathcal{S}) \rightarrow L^2(\mathcal{S})$ is defined as $(\mathcal{K}f)(s) = \int_{\mathcal{S}} k(s, s')f(s')ds'$.*
2. *The centered kernel operator $\mathcal{T} : L^2(\mathcal{S}) \rightarrow L^2(\mathcal{S})$ is defined as $\mathcal{T} := \mathcal{C}\mathcal{K}\mathcal{C}$, where \mathcal{C} is the centering operator, $\mathcal{C}f = f - \frac{1}{|\mathcal{S}|} \int_{\mathcal{S}} f(s)ds$.*

We adopt two standard assumptions: (1) \mathcal{S} is a compact metric space (e.g., the unit circle $\mathcal{S} = S^1$) such that $L^2(\mathcal{S})$ is separable (possessing a countable orthogonal basis); (2) \mathcal{K} (and thus \mathcal{T}) is Hilbert-Schmidt (i.e., it has a finite norm $\int \int |k|^2 < \infty$).

Definition 3.3 (Functional Q-statistic). *For a spatial pattern f , the Q-statistic is the inner product induced by the centered kernel operator \mathcal{K} ,*

$$Q(f) = \langle \mathcal{C}f, \mathcal{K}\mathcal{C}f \rangle = \langle f, \mathcal{T}f \rangle.$$

As noted in Supplementary Note 1, the kernel matrix $\mathbf{K} \in \mathbb{R}^{n \times n}$ serves as the discrete approximation of \mathcal{K} based on n finite samples. We can thus formally connect the functional Q to the discrete counterpart Q_n introduced in Supplementary Note 2 and Table 1. A technical caveat arises because elements of L^2 are equivalence classes of functions equal almost everywhere; evaluating $f \in L^2$ at a finite set of points (a set of measure zero) is therefore ambiguous. Since bounded continuous functions are dense in L^2 , we assume without loss of generality that f is continuous at the sampled locations \mathbf{s} .

Definition 3.4 (Finite-sample Pattern, Kernel, and Q-statistic). *Given n unique samples $s_i \in \mathcal{S}$, the finite spatial pattern derived from f is the vector $\mathbf{x} = [f(s_1), \dots, f(s_n)]^\top \in \mathbb{R}^n$. The finite spatial kernel is the matrix $\mathbf{K}_n = [k(s_i, s_j)] \in \mathbb{R}^{n \times n}$. The discrete Q-statistic is defined as $Q_n = \mathbf{x}^\top \mathbf{H} \mathbf{K}_n \mathbf{H} \mathbf{x}$, where \mathbf{H} is the centering matrix. Note that for standardized data \mathbf{z} , $Q_n \propto \mathbf{z}^\top \mathbf{K}_n \mathbf{z}$, and the scaling factor depends on the norm of f .*

It is clear from the definition that given n samples, the space of all possible spatial patterns is of dimension n . As $n \rightarrow \infty$, we have the following convergence result:

Proposition 3.1 (Q-statistic convergence). *Let (\mathcal{S}, d, μ) be a compact metric measure space with probability measure μ . Let the observation locations $\{s_i\}_{i=1}^n$ be i.i.d. samples drawn from μ . The scaled discrete Q-statistic can be formulated as a V-statistic as before,*

$$\frac{1}{n^2} Q_n(\mathbf{x}) = \frac{1}{n^2} \sum_{i=1}^n \sum_{j=1}^n \tilde{x}_i k(s_i, s_j) \tilde{x}_j,$$

where \tilde{x}_i represents the empirically centered observations. By the Strong Law of Large Numbers for V-statistics, this quantity serves as a Monte Carlo approximation of the double integral defined by the operator \mathcal{T} , converging almost surely to the functional Q-statistic

$$\frac{1}{n^2} Q_n(\mathbf{x}) = \frac{1}{n^2} \mathbf{x}^\top \mathbf{H} \mathbf{K}_n \mathbf{H} \mathbf{x} \xrightarrow{a.s.} \iint_{\mathcal{S} \times \mathcal{S}} \bar{f}(s) k(s, s') \bar{f}(s') d\mu(s) d\mu(s') = \langle f, \mathcal{T}f \rangle = Q(f),$$

where $\bar{f} = \mathcal{C}f$ is the centered function and $\mathbf{x}_i = f(s_i)$.

3.2 Spectral properties of kernel operators

The asymptotic null distribution of V-statistics, introduced in Eq. (2) of Supplementary Note 2, implies that the consistency of a Q-test is determined by the spectrum of its underlying kernel operator. In this section, we summarize key spectral properties relevant to our analysis.

Lemma 1 (Spectral decomposition of \mathcal{K}). *By assumption, the operator \mathcal{K} is self-adjoint (since $k(\cdot, \cdot)$ is symmetric) and Hilbert-Schmidt, and consequently compact. By the Spectral Theorem for compact self-adjoint operators, there exists a countable orthonormal basis of eigenfunctions $\{\phi_j\}_{j=0}^\infty$ in $L^2(\mathcal{S})$ and a corresponding sequence of real eigenvalues $\{\mu_j\}_{j=0}^\infty$ such that*

$$\mathcal{K}f = \sum_{j=0}^{\infty} \mu_j \langle f, \phi_j \rangle \phi_j.$$

The eigenvalues satisfy $|\mu_0| \geq |\mu_1| \geq \dots \rightarrow 0$ as $j \rightarrow \infty$.

Proposition 3.2 (Spectral decomposition of \mathcal{T}). *The centered operator $\mathcal{T} = \mathcal{C}\mathcal{K}\mathcal{C}$ restricts the action of \mathcal{K} to the subspace of zero-mean functions, $L_0^2(\mathcal{S}) = \{f \in L^2(\mathcal{S}) : \int_{\mathcal{S}} f = 0\}$. Its spectral properties are as follows:*

1. **Nullspace:** The constant function $\mathbf{1}$ lies in the kernel of \mathcal{T} , corresponding to an eigenvalue $\lambda_0 = 0$.
2. **Eigenvalue Interlacing:** By the Courant-Fischer Min-Max Theorem, the eigenvalues $\{\lambda_j\}$ of the projected operator \mathcal{T} are interlaced with (specifically, are less than or equal to) the eigenvalues $\{\mu_j\}$ of the uncentered operator \mathcal{K} .
3. **Translation Invariance:** If the constant function $\mathbf{1}$ is an eigenfunction of \mathcal{K} (e.g., if \mathcal{K} is translation invariant on a periodic domain), then the spectrum of \mathcal{T} is identical to that of \mathcal{K} , excluding the eigenvalue associated with the constant mode. The eigenfunctions of \mathcal{T} are simply the centered eigenfunctions of \mathcal{K} .

Proof. We prove the third statement. Assume $\mathcal{K}\mathbf{1} = \mu_c \mathbf{1}$. Let (μ, ϕ) be an eigenpair of \mathcal{K} such that $\phi \perp \mathbf{1}$ (i.e., $\phi \in L_0^2(\mathcal{S})$). Since ϕ has zero mean, $\mathcal{C}\phi = \phi$. Then,

$$\mathcal{T}\phi = \mathcal{C}\mathcal{K}\mathcal{C}\phi = \mathcal{C}\mathcal{K}\phi = \mathcal{C}(\mu\phi) = \mu\mathcal{C}\phi = \mu\phi.$$

Thus, every eigenpair of \mathcal{K} orthogonal to the constant function is preserved by \mathcal{T} . \square

Proposition 3.2 implies that centering introduces a necessary “blind spot” at frequency zero. For translation invariant kernels on periodic domains (e.g., the torus), the analysis simplifies further via the Convolution Theorem.

Lemma 2 (Spectrum of Stationary Kernels). *Let \mathcal{K} be a spatial convolution operator defined on a periodic domain (e.g., the torus \mathbb{T}^d), such that $k(s, s') = \psi(s - s')$. The eigenfunctions of \mathcal{K} are the Fourier basis functions $\{\phi_\omega(s) = e^{i\omega \cdot s}\}_{\omega \in \mathbb{Z}^d}$. The eigenvalues are given by the Fourier coefficients of the kernel profile ψ ,*

$$\lambda(\omega) = \int_S \psi(u) e^{-i\omega \cdot u} du.$$

Remark: The index ω above is discrete. On the unbounded domain $\mathcal{S} = \mathbb{R}^d$, the translation-invariant operator admits a continuous spectrum. The eigenfunctions are generalized plane waves $\{e^{i\xi \cdot s}\}_{\xi \in \mathbb{R}^d}$, and the eigenvalues are described by the continuous spectral density function $\hat{\psi}(\xi) = \int_{\mathbb{R}^d} \psi(u) e^{-i\xi \cdot u} du$. Our assumption of a compact domain \mathcal{S} (e.g., a d -dimensional torus of side length L) imposes periodic boundary conditions that restrict the admissible eigenfunctions to those satisfying $f(s) = f(s + L \cdot e_j)$. This condition discretizes the frequency domain, permitting only wave vectors on the reciprocal lattice

$$\omega \in \Lambda = \left\{ \frac{2\pi}{L} \mathbf{k} : \mathbf{k} \in \mathbb{Z}^d \right\}.$$

Consequently, the spectrum becomes a countable sampling of the continuous spectral density at these fixed lattice points: $\lambda_{\mathbf{k}} = \hat{\psi}\left(\frac{2\pi}{L} \mathbf{k}\right)$. As the domain size $L \rightarrow \infty$, the lattice becomes denser, and the discrete spectrum converges to the continuous spectral density of \mathbb{R}^d .

3.3 Consistency conditions of Q-tests on spatial patterns

We now address the central question: under what conditions can a Q-test detect *any* non-constant spatial pattern? We define a test as *universally consistent* if the test statistic is non-zero for all non-constant inputs.

Theorem 2 (Universal consistency of functional Q-test). *A Q-test based on the centered operator \mathcal{T} is consistent against all non-constant spatial patterns (i.e., $Q(f) \neq 0$ for all $f \in L_0^2(\mathcal{S}) \setminus \{0\}$) if and only if \mathcal{T} is strictly definite on the mean-zero subspace. Specifically, if $\{\lambda_j\}_{j=1}^\infty$ are the eigenvalues corresponding to non-constant eigenfunctions, we require either $\forall j, \lambda_j > 0$ (positive definite) or $\forall j, \lambda_j < 0$ (negative definite).*

Proof. Decompose $f = c\mathbf{1} + g$ where $g \in L_0^2(\mathcal{S})$. Then $Q(f) = \langle g, \mathcal{T}g \rangle = \sum_{j=1}^\infty \lambda_j |\langle g, \phi_j \rangle|^2$.

Sufficiency: If λ_j are strictly positive (or strictly negative), then $Q(f) = 0$ implies $\langle g, \phi_j \rangle = 0$ for all j . Since $\{\phi_j\}$ is a basis, $g = 0$, implying f is constant.

Necessity: The test fails if the operator exhibits either of two spectral pathologies:

1. **Blind Spots:** If $\lambda_k = 0$ for some $k \geq 1$, let $f = \phi_k$. Then $Q(f) = 0$ despite f being non-constant.
2. **Cancellation:** If there exist eigenvalues with opposite signs, say $\lambda_p > 0$ and $\lambda_q < 0$, let $f = \sqrt{|\lambda_q|} \phi_p + \sqrt{|\lambda_p|} \phi_q$. Then $Q(f) = \lambda_p |\lambda_q| + \lambda_q \lambda_p = 0$.

□

In practice, we operate on discrete data vectors $\mathbf{x} \in \mathbb{R}^n$ rather than functions. While the spectrum of the operator governs asymptotic consistency, the algebraic properties of the kernel matrix \mathbf{K}_n determine the test's power in finite samples. This distinction is particularly relevant for graph-based kernels, where an underlying continuous operator from $k(\cdot, \cdot)$ may not be explicitly defined.

Corollary 2.1 (Finite-sample detectability, Theorem 1 of Su et al. [1]). *Consider a sample of size n and a centered kernel matrix $\tilde{\mathbf{K}} = \mathbf{H} \mathbf{K}_n \mathbf{H}$. The statistic $Q_n = \mathbf{x}^\top \tilde{\mathbf{K}} \mathbf{x}$ can detect all non-constant patterns $\mathbf{x} \in \mathbb{R}^n$ (where $\mathbf{x} \neq c\mathbf{1}$) if and only if $\tilde{\mathbf{K}}$ is strictly definite on the subspace $\mathbf{1}^\perp$.*

If $\tilde{\mathbf{K}}$ is indefinite or singular on this subspace, there exists a non-empty set of “invisible” patterns $\mathcal{N} = \{\mathbf{x} \in \mathbf{1}^\perp \setminus \{0\} : Q_n = \mathbf{x}^\top \tilde{\mathbf{K}} \mathbf{x} = 0\}$ for which the test has zero power.

3.4 Spectral diagnoses of inconsistent SVG methods

As a direct application of this spectral framework, we diagnose two popular but theoretically inconsistent spatial variability tests.

Example 1: SPARK-X¹⁹ SPARK-X was developed as an extension to SPARK¹⁵ to improve scalability and robustness on sparse data. It replaces the parametric Poisson assumption with a linear kernel framework, thereby eliminating the need for iterative model fitting and avoiding potential algorithm stability issues. As detailed in Supplementary Note 2.5.1, our analysis of GLMs and GLMMs indicates that the mean-scaling factor $\hat{\mu}_0^2$ inherent in Poisson models disproportionately shrinks the test statistic for lowly expressed genes, resulting in substantial power loss. By adopting a nonparametric approach, SPARK-X effectively reverts the model to a Gaussian-like formulation, mitigating this scaling issue and restoring detection power for sparse features.

On spatial modeling, SPARK-X adopts a low-rank kernel structure for memory and runtime savings. The kernel is constructed as a sum of 11 predefined rank-2 kernels $k(s, s') = \sum_{i=1}^{11} \langle \phi_i(s), \phi_i(s') \rangle$, where $\phi_i : \mathbb{R}^2 \rightarrow \mathbb{R}^2$. Consequently, the operator has finite rank (at most 22 non-zero eigenvalues) and possesses an infinite-dimensional null space (*Blind Spots*). Any spatial pattern orthogonal to the 22 generating functions results in $Q_n = 0$. The test is therefore inconsistent, a limitation previously noted in terms of zero power by Su *et al.* [1].

This diagnosis extends to other SVG detection methods that rely on fixed effects or low-rank kernel approximations. For instance, C-SIDE¹³ utilizes spatial covariates $\mathbf{L} \in \mathbb{R}^{n \times d}$ where typically $d \ll n$, resulting a substantial null space. Similarly, methods employing Nyström approximations in GP regression sacrifice consistency for computational speed. As discussed in Supplementary Note 2.7.4, singleCellHaystack²⁴ exhibits similar behavior; its default discretization of the spatial (or low-dimensional embedding) domain into a grid (e.g., 100 points by default) imposes a low-rank constraint that also creates blind spots, especially when the sample size $n \gg 100$.

Example 2: Moran's I⁴ The spatial kernel is the adjacency matrix $\mathbf{K}_n = \mathbf{W}$ of a neighborhood graph. If the graph represents a binary indicator kernel $k(s, s') = \mathbb{I}(\|s - s'\| < r)$ on \mathbb{R}^d given a fixed radius r , then the eigenvalue spectrum is given by the Hankel transform,

$$\mu(\omega) = \left(\frac{2\pi r}{\|\omega\|} \right)^{d/2} J_{d/2}(r\|\omega\|),$$

where $J_{d/2}$ is the Bessel function of the first kind. Since the Bessel function oscillates around zero, the spectrum contains both positive values (clustering) and negative values (dispersion/checkerboard patterns), as well as roots where $\mu(\omega) = 0$. This means that Moran's I suffers from the *Cancellation* pathology defined in Theorem 2. There exist composite patterns mixing clustering and dispersion that result in $I \approx 0$, making it an inconsistent test for general spatial variability (though it remains consistent for global spatial autocorrelation).

More generally, for an arbitrary symmetric graph adjacency matrix \mathbf{W} without self-loops, the diagonal elements are zero ($W_{ii} = 0$) and $\text{Tr}(\mathbf{W}) = \sum \lambda_i = 0$. Unless $\mathbf{W} = \mathbf{0}$, the spectrum *must* contain both positive and negative eigenvalues to sum to zero, thereby invoking Corollary 2.1 and resulting in power loss. This diagnosis extends to other graph-based approaches, including Hotspot⁶, MERINGUE⁷, and BinSpect²⁰.

3.5 Power analysis and kernel design

While consistency is a binary property (a test is either consistent or it is not), statistical power is continuous. For a fixed sample size, the power of a Q-test to detect a spatial pattern f is monotonically related to the magnitude of the statistic $|Q(f)|$. Following Lemma 2, we can decompose both the kernel and the spatial pattern into their frequency components, such that $Q(f) = \sum_{\omega} |\hat{f}_{\omega}|^2 \lambda(\omega)$. In this representation, the kernel spectrum $\lambda(\omega)$ acts as a “frequency filter,” determining the sensitivity profile of the test.

3.5.1 No kernel is universally optimal

Among the class of positive definite kernels, no single kernel is universally optimal for detecting all spatial patterns. To see this, observe that scaling the kernel spectrum by a constant factor scales the test statistic and the null distribution identically (Eq. (2)), leaving the p -value unchanged. Therefore, under a fixed trace constraint (e.g., $\sum \lambda_i = C$), increasing the spectral weight $\lambda(\omega)$ at specific frequencies to prioritize certain patterns necessitates decreasing the weight at others. The choice of kernel is, hence, inherently a *design choice*: different kernels prioritize different spatial frequencies. This explains the discrepancies often observed between consistent SVG detection methods; they are simply tuned to detect different types of spatial variation.

We compare three major kernel classes by their spectral response to spatial frequencies $|\omega|$.

Example 3: Gaussian Kernel (soft low-pass filter). For the standard radial basis function $k(s, s') = \exp(-|s - s'|^2/2l^2)$, the spectrum is given by the Fourier transform of a Gaussian, which is itself a Gaussian

$$\mu(\omega) \propto \exp(-l^2\|\omega\|^2/2).$$

Since the spectral density is strictly positive for all ω , the Gaussian kernel is universally consistent. However, it acts as a soft low-pass filter with exponential decay. The sensitivity is strictly governed by the bandwidth parameter l . A large l results in rapid spectral decay, providing high power for global, low-frequency trends but near-zero power for local, high-frequency variations. Conversely, as $l \rightarrow 0$, the kernel approaches the identity matrix (white noise), distributing power equally but weakly across all frequencies.

Example 4: Graph Laplacian Kernel (high-pass filter). The unnormalized Graph Laplacian is $\mathbf{L}_n = \mathbf{D} - \mathbf{W}$. In the continuous limit, this operator converges to the negative Laplacian $-\Delta$ (Supplementary Note 1). While technically not an integral kernel operator, we can still study $-\Delta$ using spectral theory. Its eigenvalues grow quadratically with frequency,

$$\lambda(\omega) \propto \|\omega\|^2.$$

Consequently, it acts as a high-pass filter. The corresponding Q-statistic $Q_n = \mathbf{z}^\top \mathbf{L}_n \mathbf{z}$ is proportional to the Laplacian score³¹, which was first introduced and generalized for SVG testing by Govek *et al.* [32]. It measures spatial “roughness,” assigning high power to high-frequency variation and low power to smooth, global trends. This is generally the inverse of the desired behavior for detecting spatial coherence (clustering), though it effectively identifies high-frequency textures (e.g., tumor plasticity).

The Laplacian kernel is spectrally coupled to the adjacency kernel of Moran’s I. For the normalized adjacency matrix $\tilde{\mathbf{W}} = \mathbf{D}^{-1/2} \mathbf{W} \mathbf{D}^{-1/2}$, the eigenvalues relate to the normalized Laplacian $\tilde{\mathbf{L}}$ via $\lambda_i(\tilde{\mathbf{L}}) = 1 - \mu_i(\tilde{\mathbf{W}})$. Since $\mu_i(\tilde{\mathbf{W}}) \in [-1, 1]$, the Laplacian eigenvalues map to $\lambda_i(\tilde{\mathbf{L}}) \in [0, 2]$. While this linear shift resolves the indefiniteness of Moran’s I (making the operator positive semi-definite), it amplifies the high-frequency “checkerboard” modes (where $\mu \approx -1 \implies \lambda \approx 2$) while suppressing the biologically relevant clustering modes (where $\mu \approx 1 \implies \lambda \approx 0$). Note for $\tilde{\mathbf{W}}$, $Q_{\text{Lap}} = \mathbf{z}^\top \mathbf{I} \mathbf{z} - \mathbf{z}^\top \tilde{\mathbf{W}} \mathbf{z} = n + Q_{\text{Moran}}$. This suggests that Moran’s I can be viewed as a consistent (high-pass) pattern detector up to a shift correction.

Remark: Different spectral filters can be combined in arbitrary ways to generate new kernels and SVG tests. For example, SpAGFT³³ introduces an exponential transformation $\tilde{\lambda}(\omega) = e^{-\lambda(\omega)} \propto e^{-\|\omega\|^2}$ on top of the Graph Laplacian spectrum, essentially reverting back to a Gaussian kernel.

Example 5: Inverse Laplacian (polynomial low-pass filter). The Inverse Laplacian (a.k.a. CAR) kernel is defined as $\mathbf{K} = (\mathbf{I} - \rho \tilde{\mathbf{W}})^{-1}$, corresponding to the covariance of a conditional autoregressive (CAR) process with autocorrelation $\rho \in (0, 1)$ ³⁴. In the continuous limit, this kernel converges to the resolvent of the Laplacian operator, $(I - \alpha \Delta)^{-1}$. Its spectrum is given by,

$$\lambda(\omega) \propto \frac{1}{1 + \alpha \|\omega\|^2}.$$

Unlike the exponential decay of the Gaussian kernel, the CAR kernel exhibits polynomial decay (heavy-tailed). Theoretically, this is equivalent to the Matérn kernel with smoothness parameter $\nu = 0$ in \mathbb{R}^2 (or $\nu = 0.5$ in \mathbb{R}^1) via the stochastic partial differential equation, as first shown by Lindgren

et al. [35]. This heavy tail preserves significantly more power for intermediate and high-frequency patterns than the Gaussian kernel. Using the eigenvalue relation $\lambda_i(\mathbf{K}) = (1 - \rho\mu_i(\tilde{\mathbf{W}}))^{-1}$, we see that the CAR transforms the indefinite spectrum of $\tilde{\mathbf{W}}$ into a positive definite spectrum that correctly prioritizes low-frequency clustering modes ($\mu \approx 1$) while damping high-frequency checkerboard modes ($\mu \approx -1 \implies \lambda \approx 0.5$).

The limitation of Moran’s I lies in its conflation of high and low frequencies through an oscillatory spectrum. Our analysis suggests that Moran’s I can be split into two robust complementary components, the high-pass Graph Laplacian (for roughness) and the low-pass Inverse Laplacian (for smoothness). One computational advantage of this approach is sparsity. The Graph Laplacian retains the sparsity structure of the adjacency matrix, reducing the memory complexity of kernel evaluation from $O(N^2)$ for dense kernels to $O(kN)$ for k -mutual-nearest-neighbors.

3.5.2 Data-driven kernels do not guarantee better performance

Given that fixed kernels impose specific spectral priors, it is tempting to employ data-driven approaches to learn the kernel parameters or the kernel structure itself, as suggested by Svensson *et al.* [9] and Yan *et al.* [21]. Nevertheless, it is also important to distinguish the objectives of *model inference* and *hypothesis testing*. In modeling (e.g., GP regression), hyperparameter tuning is essential to minimize prediction error. In hypothesis testing, however, optimizing the kernel to maximize the test statistic on the observed data constitutes a form of “double dipping” or “p-hacking,” which can lead to inflated Type I error rates. We categorize these risks across a spectrum of model flexibility.

Because any random spatial pattern in a finite sample corresponds to infinitely many deterministic functions, it is theoretically possible to find specific kernel structure for each gene that makes any \mathbf{x} statistically significant. Therefore, gene-specific optimization is prone to overfitting. For example, tuning the Gaussian bandwidth l for each gene (as in `SpatialDE`⁹) allows the model to select a length scale that maximizes the significance of noise artifacts. Even when constrained to a single degree of freedom, such optimization may expose the kernel to the specific realization of noise, making it difficult to distinguish signal from spurious fluctuations.

Alternatively, one might optimize a set of global kernel hyperparameters across the entire dataset to avoid gene-specific overfitting. While this preserves valid error control, it biases the test toward the dominant sources of variation in the data. If the dataset is plagued by technical noise or broad structural trends, the learned kernel will prioritize these features. Biologically distinct but rare patterns, which do not align with the “majority vote” of the global parameters, may be masked. This is most common in deep learning methods such as Convolutional Neural Networks (CNNs) and Graph Convolutional Networks (GCNs). As discussed in Section 1.4, they effectively learn the kernel matrix \mathbf{K}_{conv} itself, with a specific spectrum $\text{eig}(\mathbf{K}_{\text{conv}}) = \mathcal{F}(\tilde{\mathbf{A}})$. Just as a CNN learns to detect specific visual features, a data-driven kernel acts as a matched filter, maximizing sensitivity only to patterns prioritized during training.

A prominent example is `SpaGCN`³⁶, which trains a GCN using an iterative unsupervised clustering objective and identifies SVGs via differential expression analysis between the resulting clusters. From a kernel testing perspective, this process is twofold: (1) The GCN layer aggregates data via a learnable adjacency matrix \mathbf{A} , acting as a low-pass filter that smooths expression between neighbors. (2) The clustering step constructs a discrete kernel function $k(s, s') = \mathbb{I}(\text{domain}(s) = \text{domain}(s'))$ using the learned parameters (e.g., \mathbf{A}). Since expression \mathbf{x} is used in training to learn $k(\cdot, \cdot)$, hypothesis testing here is inherently circular^{37,38}. Specifically, `SpaGCN`’s training objective maximizes the separation of gene expression profiles with all genes $\{\mathbf{x}_g\}_g$, so its SVG test prioritizes genes that align with the majority and drive the clustering.

In summary, there is no “unbiased” data-driven kernel; there is only a kernel biased by the training data and the objective function. Therefore, for general-purpose SVG discovery, a fixed, heavy-tailed kernel (like the CAR or Matérn) often provides a more robust compromise than data-driven alternatives.

Supplementary References

1. Su, J. *et al.* Mapping isoforms and regulatory mechanisms from spatial transcriptomics data with SPLISOSM. *Nature Biotechnology*, 1–12 (2026).
2. Mises, R. v. On the asymptotic distribution of differentiable statistical functions. *The Annals of Mathematical Statistics* **18**, 309–348 (1947).
3. Serfling, R. J. *Approximation theorems of mathematical statistics* (John Wiley & Sons, 2009).
4. Moran, P. A. The interpretation of statistical maps. *Journal of the Royal Statistical Society. Series B (Methodological)* **10**, 243–251 (1948).
5. Cliff, A. & Ord, J. *Spatial Processes: Models & Applications* ISBN: 9780850860818. <https://books.google.com/books?id=Mi00AAAAQAAJ> (Pion, 1981).
6. DeTomaso, D. & Yosef, N. Hotspot identifies informative gene modules across modalities of single-cell genomics. *Cell Systems* **12**, 446–456 (2021).
7. Miller, B. F., Bambah-Mukku, D., Dulac, C., Zhuang, X. & Fan, J. Characterizing spatial gene expression heterogeneity in spatially resolved single-cell transcriptomic data with nonuniform cellular densities. *Genome Research* **31**, 1843–1855 (2021).
8. Burridge, P. On the Cliff-Ord test for spatial correlation. *Journal of the Royal Statistical Society: Series B (Methodological)* **42**, 107–108 (1980).
9. Svensson, V., Teichmann, S. A. & Stegle, O. SpatialDE: identification of spatially variable genes. *Nature Methods* **15**, 343–346 (2018).
10. Chernoff, H. On the distribution of the likelihood ratio. *The Annals of Mathematical Statistics*, 573–578 (1954).
11. Hao, M., Hua, K. & Zhang, X. SOMDE: a scalable method for identifying spatially variable genes with self-organizing map. *Bioinformatics* **37**, 4392–4398 (2021).
12. Weber, L. M., Saha, A., Datta, A., Hansen, K. D. & Hicks, S. C. nnSVG for the scalable identification of spatially variable genes using nearest-neighbor Gaussian processes. *Nature Communications* **14**, 4059 (2023).
13. Cable, D. M. *et al.* Cell type-specific inference of differential expression in spatial transcriptomics. *Nature Methods* **19**, 1076–1087 (2022).
14. Wu, M. C. *et al.* Rare-variant association testing for sequencing data with the sequence kernel association test. *The American Journal of Human Genetics* **89**, 82–93 (2011).
15. Sun, S., Zhu, J. & Zhou, X. Statistical analysis of spatial expression patterns for spatially resolved transcriptomic studies. *Nature Methods* **17**, 193–200 (2020).
16. BinTayyash, N. *et al.* Non-parametric modelling of temporal and spatial counts data from RNA-seq experiments. *Bioinformatics* **37**, 3788–3795 (2021).
17. Gretton, A., Bousquet, O., Smola, A. & Schölkopf, B. *Measuring statistical dependence with hilbert-schmidt norms* in *Proceedings of the 16th international conference on Algorithmic Learning Theory* (2005), 63–77.
18. Gretton, A. *et al.* A kernel statistical test of independence. *Advances in Neural Information Processing Systems* **20** (2007).
19. Zhu, J., Sun, S. & Zhou, X. SPARK-X: non-parametric modeling enables scalable and robust detection of spatial expression patterns for large spatial transcriptomic studies. *Genome Biology* **22**, 184 (2021).
20. Dries, R. *et al.* Giotto: a toolbox for integrative analysis and visualization of spatial expression data. *Genome Biology* **22**, 78 (2021).
21. Yan, G., Hua, S. H. & Li, J. J. Categorization of 34 computational methods to detect spatially variable genes from spatially resolved transcriptomics data. *Nature Communications* **16**, 1141 (2025).
22. Edsgård, D., Johnsson, P. & Sandberg, R. Identification of spatial expression trends in single-cell gene expression data. *Nature Methods* **15**, 339–342 (2018).

23. Baddeley, A., Turner, R., *et al.* Package ‘spatstat’. *The Comprehensive R Archive Network ()* **146** (2014).
24. Vandenbon, A. & Diez, D. A clustering-independent method for finding differentially expressed genes in single-cell transcriptome data. *Nature Communications* **11**, 4318 (2020).
25. Cable, D. M. *et al.* Robust decomposition of cell type mixtures in spatial transcriptomics. *Nature Biotechnology* **40**, 517–526 (2022).
26. Yu, J. & Luo, X. Identification of cell-type-specific spatially variable genes accounting for excess zeros. *Bioinformatics* **38**, 4135–4144 (2022).
27. Yu, S. & Li, W. V. spVC for the detection and interpretation of spatial gene expression variation. *Genome Biology* **25**, 103 (2024).
28. Su, H., Wu, Y., Chen, B. & Cui, Y. STANCE: a unified statistical model to detect cell-type-specific spatially variable genes in spatial transcriptomics. *Nature Communications* **16**, 1793 (2025).
29. Shang, L., Wu, P. & Zhou, X. Statistical identification of cell type-specific spatially variable genes in spatial transcriptomics. *Nature Communications* **16**, 1059 (2025).
30. Wang, Z. *et al.* A unified framework for identification of cell-type-specific spatially variable genes in spatial transcriptomic studies. *Proceedings of the National Academy of Sciences* **122**, e2503952122 (2025).
31. He, X., Cai, D. & Niyogi, P. Laplacian score for feature selection. *Advances in Neural Information Processing Systems* **18** (2005).
32. Govek, K. W., Yamajala, V. S. & Camara, P. G. Clustering-independent analysis of genomic data using spectral simplicial theory. *PLoS Computational Biology* **15**, e1007509 (2019).
33. Chang, Y. *et al.* Graph Fourier transform for spatial omics representation and analyses of complex organs. *Nature Communications* **15**, 7467 (2024).
34. Su, J. *et al.* Smoother: a unified and modular framework for incorporating structural dependency in spatial omics data. *Genome Biology* **24**, 291 (2023).
35. Lindgren, F., Rue, H. & Lindström, J. An explicit link between Gaussian fields and Gaussian Markov random fields: the stochastic partial differential equation approach. *Journal of the Royal Statistical Society Series B: Statistical Methodology* **73**, 423–498 (2011).
36. Hu, J. *et al.* SpaGCN: Integrating gene expression, spatial location and histology to identify spatial domains and spatially variable genes by graph convolutional network. *Nature Methods* **18**, 1342–1351 (2021).
37. Zhang, J. M., Kamath, G. M. & David, N. T. Valid post-clustering differential analysis for single-cell RNA-Seq. *Cell Systems* **9**, 383–392 (2019).
38. Song, D. *et al.* *Synthetic control removes spurious discoveries from double dipping in single-cell and spatial transcriptomics data analyses* in *International Conference on Research in Computational Molecular Biology* (2025), 400–404.